

1 **Semi-quantitative understanding of source contribution to nitrous**
2 **acid (HONO) based on 1-year continuous observation at the**
3 **SORPES station in eastern China**

4
5 Yuliang Liu^{1,2}, Wei Nie^{1,2*}, Zheng Xu^{1,2}, Tianyi Wang^{1,2}, Ruoxian Wang^{1,2},
6 Yuanyuan Li^{1,2}, Lei Wang^{1,2}, Xuguang Chi^{1,2}, and Aijun Ding^{1,2}

7
8 ¹Joint International Research Laboratory of Atmospheric and Earth System Sciences, School
9 of Atmospheric Sciences, Nanjing University, Nanjing, Jiangsu Province, China

10 ² Collaborative Innovation Center of Climate Change, Jiangsu Province, China

11
12 **Abstract**

13
14 Nitrous acid (HONO), an important precursor of the hydroxyl radical (OH), has been
15 long-standing recognized to be of significance to atmospheric chemistry, but its
16 sources are still debate. In this study, we conducted continuous measurement of
17 HONO from November 2017 to November 2018 at the SORPES station in Nanjing of
18 eastern China. The yearly average mixing ratio of observed HONO was 0.69 ± 0.58
19 ppb, showing a larger contribution to OH relative to ozone with a mean net OH
20 production rate of 0.59 ppb/h. To estimate the effect of combustion emissions of
21 HONO, the emitted ratios of HONO and NO_x were derived from 55 fresh plumes
22 (NO/NO_x > 0.85), with a mean value of 0.79%. During the nighttime, the chemistry of
23 HONO was found to depend on RH, and heterogeneous reaction of NO₂ on aerosol
24 surface was presumably responsible for HONO production. The average nighttime
25 NO₂-to-HONO conversion frequency (C_{HONO}) was determined to be 0.0055 ± 0.0032
26 h⁻¹ from 137 HONO formation cases. The missing source of HONO around noontime
27 seemed to be photo-induced with an average P_{unknown} of 1.02 ppb h⁻¹, based on a
28 semiquantitative HONO budget analysis. An over-determined system of equations
29 was applied to obtain the monthly variations in nocturnal HONO sources. Except for
30 burning-emitted HONO (approximately 23% of total measured HONO), the
31 contribution of heterogeneous formation on ground surfaces was an approximately

32 constant proportion of 36% throughout the year. The soil emission revealed clear
33 seasonal variation, and contributed up to 40% of observed HONO in July and August.
34 A higher propensity for generating HONO on aerosol surface occurred in heavily
35 polluted period (about 40% of HONO in January). Our results highlight
36 ever-changing contributions of HONO sources, and encourage more long-term
37 observations to evaluate the contributions from varied sources.

38

39 **1. Introduction**

40

41 Nitrous acid (HONO) is a vital constituent of nitrogen cycle in the atmosphere, first
42 observed in the field by Perner and Platt (1979). The concentrations of HONO varied
43 from dozens of ppt in remote regions (Villena et al., 2011b;Meusel et al., 2016) to
44 several ppb in polluted urban regions (Yu et al., 2009;Tong et al., 2015). The
45 photolysis of HONO (R1) has been long standing as a momentous source of the
46 hydroxyl radicals (OH) especially during the early morning when other OH sources
47 are minor (Platt et al., 1980;Alicke, 2002, 2003). Even during the daytime, recent
48 studies have recognized the photolysis of HONO as a potentially stronger contributor
49 to daytime OH radicals than that of O₃ (Kleffmann, 2005;Elshorbany et al., 2009;Li et
50 al., 2018). Meanwhile, HONO has been found to affect adversely human health (Jarvis
51 et al., 2005;Sleiman et al., 2010).

52

53 Although the significance of HONO has been given much weight, the sources of
54 ambient HONO are complicated and have been debated for decades. HONO can be
55 emitted from combustion, including vehicle exhaust, industrial exhaust and biomass
56 burning (Table 1).Tunnel experiments with tests for different engine types have
57 determined an emission ratio of HONO/NO_x for traffic source, ranged in 0.3-0.8%
58 (Kirchstetter et al., 1996;Kurtenbach et al., 2001). The release from soil nitrite
59 through acidification reaction and partitioning is considered to be another primary
60 source of atmospheric HONO (Su et al., 2011). Soil nitrite could come from
61 biological nitrification and denitrification processes (Canfield et al., 2010;Oswald et
62 al., 2013), or be enriched via reactive uptake of HONO from the atmosphere

63 (VandenBoer et al., 2014a;VandenBoer et al., 2014b). In addition to direct emissions,
64 the vast majority of HONO is produced chemically. The recombination of NO and
65 OH (R3) is the main homogeneous reaction for supplying HONO (Pagsberg et al.,
66 1997;Atkinson, 2000), whose contribution may be significant under conditions of
67 sufficient reactants at daytime. During the nighttime, with low OH concentrations,
68 other larger sources, *i.e.* heterogeneous reactions of NO₂ on various surfaces, are
69 required to explain elevated mixing levels of HONO. Laboratory studies indicate that
70 NO₂ can be converted to HONO on humid surfaces (R4), being first order in NO₂ and
71 depending on various parameters including the gas phase NO₂ concentration, the
72 surface water content, and the surface area density (Kleffmann et al.,
73 1998;Finlayson-Pitts et al., 2003). Besides, heterogeneous reduction of NO₂ with
74 surface organics (R5) is proposed to be another effective pathway to generate HONO
75 (Ammann et al., 1998;Ammann et al., 2005;Aubin and Abbatt, 2007), observed in
76 freshly emitted plumes with high concentrations of NO_x and BC (Xu et al., 2015).
77 Notably this reaction rate is drastically reduced after the first few seconds due to
78 consumption of the reactive surfaces (Kalberer et al., 1999;Kleffmann et al., 1999),
79 but this reaction could be strongly enhanced by light on photo-activated surface
80 (George et al., 2005;Stemmler et al., 2006;Stemmler et al., 2007). During the daytime,
81 heterogeneous HONO formation from the photolysis of adsorbed nitric acid (HNO₃)
82 and particulate nitrate (NO₃⁻) at UV wavelengths has been found in experiments and
83 observations (Zhou et al., 2003;Zhou et al., 2011;Ye et al., 2016;Ye et al., 2017).
84 Heterogeneous processes are typically considered as the primary sources of HONO in
85 many regions yet are the most poorly understood. For NO₂ conversion to HONO on
86 surfaces (R4,R5), the uptake coefficients of NO₂ derived from different experiments
87 vary from 10⁻⁹ to 10⁻² (Ammann et al., 1998;Kirchner et al., 2000;Underwood et al.,
88 2001;Aubin and Abbatt, 2007;Zhou et al., 2015). The key step to determine the
89 uptake of NO₂ or the reaction rate is still ill-defined, and we are also not certain if and
90 how the ambient natural surfaces can be reactivated by radiation. Furthermore, it has
91 become a main concern to compare the contributions of ground and aerosol surfaces
92 to HONO formation. It is so far, not well explained for the observed HONO,

93 especially during daytime. Large unknown sources of HONO were identified by many
94 studies (Su et al., 2008b;Sörgel et al., 2011;Michoud et al., 2014;Lee et al., 2016).

95

96 Benefitting from more and more studies, particularly the observations under different
97 environments (Lammel and Cape, 1996;Li et al., 2012), understanding of HONO
98 chemistry in the atmosphere has been greatly improved during the last decade.
99 However, most HONO observations were short-term campaigns with studies ranging
100 from several weeks to several months. For example, Reisinger (2000) found a linear
101 correlation between the HONO/NO₂ ratio and aerosol surface density in the polluted
102 winter atmosphere; and Nie et al. (2015) showed the influence of biomass burning
103 plumes on HONO chemistry, according to observed data during late April–June 2012;
104 while Wong et al. (2011) believed that NO₂ to HONO conversion on the ground was
105 the dominant source of HONO by analyzing vertical profiles from 15 August to 20
106 September in 2006. Moreover, a theory that HONO from soil emission explained the
107 strength and diurnal variations of the missing source has been presented by Su et al.
108 (2011) based on data measured from 23 to 30 October 2004. In case the HONO
109 sources possibly exhibit temporal variability, especially seasonal differences, it is
110 challenging to draw a full picture on the basis of these short-term observations. More
111 than a year of continuous observation is needed, yet rather limited.

112

113 The Yangtze River Delta (YRD) is one of the most developed regions in eastern
114 China. Rapid urbanization and industrialization have induced severe air pollution over
115 the last three decades, particularly high concentrations of reactive nitrogen (Richter et
116 al., 2005;Rohde and Muller, 2015), including HONO (Wang et al., 2013;Nie et al.,
117 2015). In this study, we [conducted HONO observations continuously from November
118 2017 to November 2018](#), at the Station for Observation Regional Processes and the
119 Earth System (SORPES), located in the western part of the YRD, a place that can be
120 influenced by air masses from different source regions of anthropogenic emissions,
121 biomass burning, dust and biogenic emissions (Ding et al., 2013;Ding et al., 2016).
122 Our one-year observation showed well-defined diurnal patterns and obvious season

123 variations of HONO concentrations at relatively high levels. We discussed the
124 potential mechanism of HONO production based upon semiquantitative analysis and
125 correlation studies, and paying special attention to changes in major sources of
126 HONO during different seasons.

127

128 **2. Methodology**

129

130 ***2.1. Study site and instrumentation***

131

132 Continuously observations was conducted at the SORPES station at the Xianlin
133 Campus of Nanjing University (118°57'E, 32°07'N), located in the northeast suburb
134 of Nanjing, China, from November 2017 to November 2018 (Fig. S1). The easterly
135 prevailing wind and synoptic condition makes it a representative background site of
136 Nanjing and a regional downwind site of the city cluster in the YRD region. Detailed
137 descriptions for the station can be found in previous studies (Ding et al., 2013;Ding et
138 al., 2016).

139

140 HONO was measured with a commercial long path absorption photometer instrument
141 (QUMA, Model LOPAP-03). The ambient air was sampled in two similar
142 temperature controlled stripping coils in series using a mixture reagent of 100 g
143 sulfanilamide and 1 L HCl (37% volume fraction) in 9 L pure water. In the first
144 stripping coil, all of the HONO and a fraction of interfering substances were absorbed
145 into solution, and the remaining interfering species (NO₂, HNO₃, HO₂NO₂, PAN, etc.)
146 were absorbed in the second stripping coil. After adding a reagent of 0.8 g
147 N-naphtylethylenediamine-dihydrochloride in 8 L pure water to both coils, colored azo
148 dye was formed in the solutions from 2 stripping coils, which were then separately
149 detected via long path absorption in special Teflon tubing. The **real** HONO signal was
150 the difference between the signals in the two channels **to minimize the measurement**
151 **interferences**. Further details can be found in (Heland et al., 2001;Kleffmann et al.,
152 2006). To correct for the small drifts in instrument's baseline, compressed air was
153 sampled every 12 h (flow rate: 1 L/min) to make zero measurement. A span check

154 was made using 0.04 mg/m³ nitrite (NO₂⁻) solution each two weeks with a flow rate of
155 0.28 ml/min. The time resolution, detection limit, accuracy of the measurement was
156 10 min, 10 pptv, and 10%, respectively.

157

158 The NO and NO₂ levels were measured using a chemiluminescence instrument (TEI,
159 model 42i) coupled with a highly selective photolytic converter (Droplet
160 Measurement Technologies, model BLC), and the analyzer had a detection limit of 50
161 pptv for an integration time of 5 min, with precision of 4% and an uncertainty of 10%
162 (Xu et al., 2013). O₃ and CO were measured continuously using Thermo-Fisher
163 Scientific TEI 49i and TEI 48i. The fine particle mass concentration (PM_{2.5}) was
164 continuously measured with a combined technique of light scattering photometry and
165 beta radiation attenuation (Thermo Scientific SHARP Monitor Model 5030). Water
166 soluble aerosol ions (NO₃⁻, SO₄²⁻, NH₄⁺ etc.) and ammonia (NH₃) were measured by a
167 Monitor for Aerosols and Gases in ambient Air (designed and manufactured by
168 Applikon Analytical B.V., the Netherlands) with a PM_{2.5} cyclone inlet, in a time
169 resolution of 1 hr. The size distribution of submicron particles (6-820 nm) is measured
170 with a DMPS (differential mobility particle sizer) constructed at the University of
171 Helsinki in Finland. Meteorological measurements including relative humidity (RH),
172 wind speed, wind direction, and air temperature were recorded by Automatic Weather
173 Station (CAMPEEL co., AG1000). UVB total radiation was measured by UVB
174 radiometer (UVS-B-T UV Radiometer, KIPP & ZONEN).

175

176 ***2.2. TUV model and OH estimate***

177

178 The Tropospheric Ultraviolet and Visible (TUV) Radiation Model
179 (<http://www.acd.ucar.edu/TUV>) was adopted to compute the photolysis frequencies,
180 which is most probably accurate in clean and cloudless days. The pivotal parameters
181 of this model were inputted as follows: the ozone density was measured by Total
182 Ozone Mapping Spectrometer (<http://toms.gsfc.nasa.gov/teacher/ozoneoverhead.html>);
183 the typical single scattering albedo (SSA) and Ångström exponent (Alpha) were 0.93
184 and 1.04 (Shen et al., 2018); The mean value of optical depth (AOD) at 550nm was

185 0.640, derived following an empirical relationship with PM_{2.5} in Nanjing (Shao et al.,
 186 2017). To reduce the error of model, we used observed UVB to correct simulated
 187 results (J_{mod}) by Eq. (1). The daytime OH concentration was calculated by applying
 188 the linear fitting formula (Eq. 2) that obtained from correlations of measured OH
 189 concentrations with simultaneously observed $J(\text{O}^1\text{D})$, suggested by Rohrer and
 190 Berresheim (2006). The coefficient a reflects the general chemical conditions (e.g.
 191 NO_x or VOCs) at the selected place for research, the exponent b represents the
 192 combined effects of all photolytic processes on OH, and the parameter c counts the
 193 light-independent OH sources. The values of a and b in Eq. (2) are adopted from the
 194 study in the Pearl River Delta (Lu et al., 2012). The value of c is set to $1.0 \times 10^6 \text{ cm}^{-3}$, a
 195 typical nighttime OH concentration in urban areas of China (Li et al., 2012; Lu et al.,
 196 2014). The calculated OH concentrations around noon were in the range of
 197 $0.15\text{-}1.6 \times 10^7 \text{ cm}^{-3}$, comparable to observations in Chinese urban atmospheres (Lu et
 198 al., 2012; Lu et al., 2013).

199

$$200 \quad J = \frac{\text{UVB}_{\text{obs}}}{\text{UVB}_{\text{mod}}} J_{\text{mod}} \quad (1)$$

$$201 \quad [\text{OH}] = a \times (J(\text{O}^1\text{D}) / 10^{-5} \text{ s}^{-1})^b + c \quad (2)$$

(a = $5.6 \times 10^6 \text{ cm}^{-3}$, b = 0.68, c = $1.0 \times 10^6 \text{ cm}^{-3}$)

202

203 3. Results

204

205 3.1. Observation overview

206

207 We carried out continuous measurements for HONO at SORPES station in the
 208 northeast suburb of Nanjing from November 2017 to November 2018 with a mean
 209 measured ambient HONO mixing level of 0.69 ± 0.58 ppb (Fig. S2), within the range
 210 of those in or in the vicinity of mega cities (Table 2). Fig.1 shows the seasonal pattern
 211 of HONO and related parameters. The highest concentration of HONO was found in
 212 winter (1.04 ± 0.75 ppb), followed by spring (0.68 ± 0.48 ppb), autumn (0.66 ± 0.53
 213 ppb) and summer (0.45 ± 0.37 ppb). Such seasonal variations in Nanjing are aligned
 214 with that in Beijing (Hendrick et al., 2014), and are somewhat similar to those in Jinan

215 (Li et al., 2018), where the highest levels occurred in winter and the lowest levels
216 occurred in autumn, but these variations are different from those in Hongkong (Xu et
217 al., 2015) where the highest and lowest values of HONO appeared in autumn and
218 spring, respectively. The important point is that the seasonality of HONO coincides
219 with that of NO_x (or NO_2), which is believed to be the main precursor of HONO, in
220 current studies.

221

222 The HONO to NO_x ratio or the HONO to NO_2 ratio has been used extensively in
223 previous researches to characterize the HONO levels and to indicate the extent of
224 heterogeneous conversion of NO_2 to HONO, since it is less influenced by convection
225 or transport processes than the individual concentration (Lammel and Cape,
226 1996; Stutz et al., 2002). When a large proportion of HONO comes from direct
227 emissions, the value of HONO/NO_2 usually becomes larger, falsely implying the
228 strong formation of HONO from NO_2 , however, the freshly emitted air masses
229 generally have the lowest HONO/NO_x ratio, meaning that HONO/NO_x behaves better
230 than HONO/NO_2 in a way. As shown in Fig. 1(b), the low value of HONO/NO_x in
231 winter is attributed to heavy emissions because we see high mixing ratios of NO
232 during this cold season (Fig. 1c), the reasons for two peaks of HONO/NO_x in spring
233 and summer will be discussed in sections 3.3, 3.4 and 4.

234

235 All daily changes of HONO concentration in different seasons closely resemble a
236 cycle where HONO peaks in the early morning, and then decreases to the minimum [in](#)
237 [the late afternoon](#), following the diurnal trend of NO_x (Fig. 2). The daily variations of
238 HONO in Nanjing are like those seen in other urban areas (Villena et al., 2011a; Wang
239 et al., 2013; Michoud et al., 2014; Lee et al., 2016), but differ from observations on the
240 roadside (Rappenglück et al., 2013; Xu et al., 2015). At night, the mixing ratio of
241 HONO increases rapidly in the first few hours and then stabilizes (in spring and
242 summer) or gradually climbs to its peak in the morning rush hour (in winter and
243 autumn). The accumulation during nighttime hours suggests a significant production
244 of HONO exceeding the dry deposition of HONO. As the sun rises, the HONO sink

245 will be strengthened by photolysis and the vertical mixing processes, resulting that the
246 peak times of the diurnal patterns of HONO concentration varies in different seasons.
247 During the daytime, the rate of HONO abatement is rapid before noon and then
248 becomes progressively until HONO concentration falling to the minimum. Given that
249 the photolytic lifetime of HONO is about 10-20 min at the midday (Stutz et al., 2000),
250 the considerable HONO concentration during daytime indicates the existence of
251 strong production of HONO.

252

253 From the daily variations of the HONO to NO_x ratio, we can further understand the
254 behavior of HONO in the atmosphere. HONO/NO_x is regularly enhanced quickly
255 before midnight then reaches a maximum during the latter half of the night.
256 According to Stutz et al. (2002), the highest HONO/NO_x (or HONO/NO₂) is defined
257 by the balance between production and loss of HONO at each night, the conditions
258 affecting the highest achievable ratio at nighttime will be discussed in section 3.3.
259 What's interesting here is the peak of the HONO/NO_x ratio in the midday sun in
260 spring, summer and autumn, and even in winter, the ratio doesn't decline but remains
261 stationary before and at noon. If the HONO sources during daytime are consistent
262 with those at night, the minimum HONO/NO_x ratios should occur at noon due to the
263 intense photochemical loss of HONO. Therefore, there must be additional sources of
264 HONO during daytime (e.g. R3). The increase of HONO/NO_x with solar radiation
265 (e.g., UVB) is found in both diurnal and seasonal variations, indicating that these
266 daytime sources have a relationship with the intensity of solar radiation. We will
267 further discuss the potential daytime sources of HONO in section 3.4.

268

269 The elevated mixing ratio of HONO presents an efficient source of OH radicals
270 during daytime in Nanjing. We calculate the net OH production rate from HONO, i.e.
271 P_{OH}(HONO), using Eq. (3) (Li et al., 2018). For comparison, the OH production rate
272 from ozone photolysis, P_{OH}(O₃), is derived from Eq. (4). Based on Alicke et al. (2002)
273 and Alicke (2003), only part of the O(¹D) atoms, formed by the photolysis of O₃ at
274 wavelengths below 320 nm (R7), can produce OH radicals by reacting with water (R8)

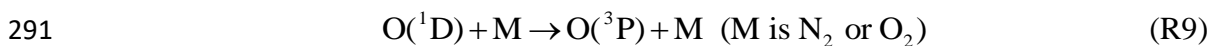
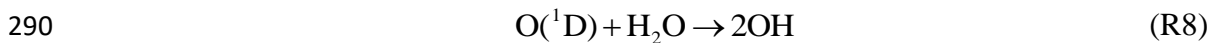
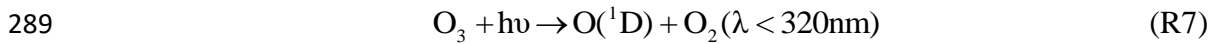
275 in the atmosphere, so we use the absolute water concentration, which can be derived
 276 from relative humidity and temperature, to calculate the branching ratio of O(¹D)
 277 (ϕ_{OH}) between R8 and R9. The reaction rate of O(¹D) with O₂ is 4.0×10^{-11} cm³
 278 molecules⁻¹ s⁻¹ and the reaction rate of O(¹D) with N₂ is 3.1×10^{-11} cm³ molecules⁻¹
 279 s⁻¹ (Seinfeld and Pandis, 2016). In addition to the two mechanisms mentioned above,
 280 there are other pathways to generate primary OH radicals: the photolysis of aldehydes,
 281 mainly HCHO, can form HO₂ radicals, and then converting to OH radicals by reacting
 282 with NO; the reactions of ozone with alkenes produce OH radicals directly; the
 283 ozonolysis of alkenes and nighttime reactions of NO₃ radicals with alkenes can also
 284 be net sources of OH radicals (Finlayson-Pitts and Pitts, 2000; Seinfeld and Pandis,
 285 2016).

286

$$287 \quad P_{OH}(HONO) = J(HONO)[HONO] - k_{NO+OH}[NO][OH] - k_{HONO+OH}[HONO][OH] \quad (3)$$

$$288 \quad P_{OH}(O_3) = 2J(O^1D)[O_3]\phi_{OH} \quad (4)$$

$$\phi_{OH} = k_8[H_2O] / (k_8[H_2O] + k_9[M])$$



292

293 Fig. 3 shows that the diurnal peak of OH production rate from HONO is usually found
 294 in the late morning, caused by the combined effects of HONO concentration and its
 295 photolysis frequency and the seasonal peak of P_{OH}(HONO) occurs in spring for the
 296 same reason. P_{OH}(O₃), coinciding with the trend of J(O¹D), is highest around noon at
 297 daily time scale and is highest in summer at seasonal time scale, respectively.
 298 Significantly, the photolysis of HONO produce more OH than that of ozone
 299 throughout the daytime in winter, spring. In summer and autumn, the contribution of
 300 HONO to OH is greater in the early morning, and although the photolysis of ozone
 301 contributes more OH at noon, the role of HONO is considerable. Overall, the average

302 P_{OH}(HONO) during 8:00-16:00 LT is 0.59 ppb/h, and the mean value of P_{OH}(O₃) is
303 0.41 ppb/h. The impressive role of HONO in the atmospheric oxidizing capacity
304 should benefit photochemical ozone production (Ding et al., 2013; Xu et al., 2017; Xu
305 et al., 2018), new particle formation (Qi et al., 2015) and secondary aerosol formation
306 (Xie et al., 2015; Sun et al., 2018) in Nanjing, the western YRD region.

307

308 ***3.2. Direct emissions of HONO from Combustion***

309

310 As mentioned above, the good correlation of HONO with NO_x (Fig. 4a) and the
311 similar patterns of HONO and NO_x, particularly sharply increasing together in the
312 fresh plumes, in which the NO/NO_x ratios are usually very high (Fig. S1), indicate the
313 presence of direct combustion emission of HONO, which need to be deducted when
314 analyzing the secondary formation of HONO. The SORPES station are influenced by
315 air masses from both industries and vehicles (Ding et al., 2016), the traffic emission
316 factor investigated in other experiments cannot be used straightly; thus, we derive the
317 emitted HONO/NO_x ratio according the method of Xu et al. (2015), and the following
318 criteria are adopted to select fresh plumes: (a) NO_x>40ppbv; (b) $\Delta\text{NO}/\Delta\text{NO}_x > 0.85$;
319 (c) good correlation between HONO and NO_x ($r > 0.9$); (d) short duration of plumes
320 ($\leq 2\text{h}$); and (e) UVB $\leq 0.01 \text{ W/m}^2$. Then, the slopes of HONO to NO_x in selected
321 plumes were considered as the emission ratios in our study.

322

323 Within the one-year dataset, we select 55 freshly emitted plumes satisfying the criteria
324 above (Table S1), of which 20 air masses were found in the morning and evening rush
325 hours; the derived $\Delta\text{HONO}/\Delta\text{NO}_x$ ratios vary from 0.26% to 1.91% with a mean
326 value of $0.79\% \pm 0.36\%$. Many factors, such as the amount of excess oxygen; the types
327 of fuel used (gasoline, diesel, coal); if engines are catalyst-equipped, and if engines
328 are well-maintained, could result in variances in these ratios. Additionally, the rapid
329 heterogeneous reduction of NO₂ on synchronously emitted BC can also raise the value
330 of $\Delta\text{HONO}/\Delta\text{NO}_x$ (Xu et al., 2015). For our study, an average emission factor of
331 0.79% is deployed to evaluate the emission contribution of HONO (Eq.5), which is
332 abbreviated as HONO_{emis}.

333

$$334 \quad \text{HONO}_{\text{emis}} = \text{NO}_x \times 0.0079 \quad (5)$$

$$335 \quad \text{HONO}_{\text{corr}} = \text{HONO} - \text{HONO}_{\text{emis}} \quad (6)$$

336

337 Combustion emissions contribute an average of 23% of total measured HONO
338 concentrations at night (Fig. 4b), with a maximum $\text{HONO}_{\text{emis}}/\text{HONO}$ value of 32% in
339 winter and a minimum $\text{HONO}_{\text{emis}}/\text{HONO}$ value of 18% in summer. We then get the
340 corrected observed HONO ($\text{HONO}_{\text{corr}}$) by Eq.(6) for further analysis. The slope of the
341 fitted line for HONO and NO_x is 1.62%, higher than emission ratio 0.79% (Fig. 4a),
342 and almost 80% of HONO is from $\text{HONO}_{\text{corr}}$ that is not affected by emissions (Fig.
343 4b). These imply significant secondary formation of HONO in the atmosphere.

344

345 **3.3. Heterogeneous conversion of NO_2 to HONO during nighttime**

346

347 **3.3.1. The NO_2 -to-HONO conversion rate (C_{HONO})**

348

349 In addition to emissions, heterogeneous reaction of NO_2 on surfaces (R4, R5) is
350 believed to be the major formation pathways of nocturnal HONO. Thus, the
351 NO_2 -to-HONO conversion rate is calculated from Eq. (5) (Alicke et al., 2002; Alicke,
352 2003; Wentzell et al., 2010), where NO_2 is adopted to scale HONO to reduce the
353 dilution influence according to Su et al. (2008a). Similar to HONO/NO_x (Fig. 2), the
354 nighttime $\text{HONO}_{\text{corr}}/\text{NO}_2$ ratio rises from the lowest value and then reaches a
355 quasi-stable state, meaning that C_{HONO} can actually be used to assess how quickly
356 $\text{HONO}_{\text{corr}}/\text{NO}_2$ can increase to its equilibrium.

357

$$358 \quad C_{\text{HONO}} = \frac{\frac{[\text{HONO}_{\text{corr}}]_{(t_2)} - [\text{HONO}_{\text{corr}}]_{(t_1)}}{[\text{NO}_2]_{(t_2)} - [\text{NO}_2]_{(t_1)}}}{t_2 - t_1} \quad (7)$$

359

360 Following the method of Xu et al. (2015) and Li et al. (2018), 137 cases in which
361 $\text{HONO}_{\text{corr}}/\text{NO}_2$ increased almost linearly from 18:00 to 24:00 each night are selected,
362 and the slope fitted by the least linear regression for $\text{HONO}_{\text{corr}}/\text{NO}_2$ against time is

363 just the conversion frequency of NO₂ to HONO. The derived values of C_{HONO} vary
364 from 0.0043±0.0017 h⁻¹ in winter to 0.0066±0.0040 h⁻¹ in summer, with an average
365 value of 0.0055±0.0032 h⁻¹, which is in the range (0.044-0.014 h⁻¹) shown by other
366 studies in urban and suburban sites (Fig. 5). Noting that C_{HONO} assumes all the
367 increase of HONO_{corr}/NO₂ is caused by the conversion of NO₂, excluding other
368 possible sources of HONO (e.g. soil nitrite); and the computed C_{HONO} is the net
369 NO₂-to-HONO conversion rate since the measured HONO_{corr} has already taken the
370 sinks of HONO (mainly deposition) into account. Considering the uncertainties of
371 C_{HONO}, utilizing C_{HONO} directly to analyze the mechanism of HONO formation
372 **thoroughly** may not be appropriate, but it could be attemptable to facilitate the
373 parameterizations for HONO production in air quality models by C_{HONO} **when the**
374 **chemical mechanisms are not clear yet.**

375

376 ***3.3.2. RH dependence of HONO chemistry***

377

378 It appears that NO₂ hydrolysis on humid surfaces (R4), having a first order
379 dependence on NO₂ (Jenkin et al., 1988;Ackermann, 2000;Finlayson-Pitts et al.,
380 2003), is influenced by the surface absorbed water (Kleffmann et al.,
381 1998;Finlayson-Pitts et al., 2003), although the exact mechanisms are still unknown.
382 In the studies of Stutz et al. (2002) and Stutz et al. (2004), the pseudo steady state of
383 HONO/NO₂, where this ratio is at a maximum **at nighttime**, is presumed to be a
384 balance between the production of HONO from NO₂ and the loss of HONO on
385 surfaces, and the highest HONO/NO₂ is determined by the ratio of the reactive uptake
386 coefficients for each process. Scatter plot of HONO_{corr}/NO₂ against relative humidity
387 in our study are illustrated in Fig. 6. **To eliminate as much influence of other factors**
388 **as possible**, the average of the 6 highest HONO_{corr}/NO₂ values in each 5% RH interval
389 is calculated, according to Stutz et al. (2004). The phenomenon that HONO_{corr}/NO₂
390 first increases and then decreases with an increasing RH in Fig. 6(a) was also
391 observed by other studies (Hao et al., 2006;Yu et al., 2009;Li et al., 2012;Wang et al.,
392 2013). The dependencies of HONO_{corr}/NO₂ on RH and the possible reasons or
393 mechanisms are discussed as follows. **Even at the lowest measured RH of 18%, the**

394 absolute moisture content in the atmosphere is still greater than 10^3 ppm in our study,
395 which is quite abundant to react with NO_2 , but the $\text{HONO}_{\text{corr}}/\text{NO}_2$ ratio is quite small
396 and remains unchanged when RH is below 45%, indicating that the NO_2 to HONO
397 conversion efficiency should be determined by water covering the surfaces, rather
398 than by the amount of water in the air.

399

400 It has been reported that surfaced absorbed water depends on RH values, and the
401 dependences vary for different material surfaces of the ground, but generally follow
402 the shape of a BET isotherm (Lammel, 1999;Saliba et al., 2001;Sumner et al., 2004).
403 The number of mono-layers of water increases slowly from zero to 2-4, accompanied
404 by RH from zero to a turning point, and the water coverage grows dramatically (up to
405 10-100 mono-layers) once RH exceeds the turning point (Finlayson-Pitts et al., 2003).
406 Fig. 6(a) shows the case where the surface for NO_2 converting to HONO is dominated
407 by the ground, the $\text{HONO}_{\text{corr}}/\text{NO}_2$ increases along with RH when RH is less than 75%,
408 which can be explained by the reaction of NO_2 to generate HONO on wet surfaces.
409 However, a negative correlation between $\text{HONO}_{\text{corr}}/\text{NO}_2$ and RH is found when RH is
410 over 75%, presumably because the rapidly growing aqueous layers of the ground
411 surface lead to efficient uptake of HONO and make the surface less accessible or less
412 reactive for NO_2 . Hence, the RH turning point for absorbed water on ground surfaces
413 is perhaps around 75% for our observation, within the range of results from
414 experiments on various surfaces (70-80% RH) (Lammel, 1999;Saliba et al.,
415 2001;Sumner et al., 2004). Once RH exceeds 95%, the reaction surface is
416 asymptotically approaching the state of water droplet, where the quite limited
417 formation of HONO and the extremely impactful loss of HONO will result in a
418 dramatic decline of the $\text{HONO}_{\text{corr}}/\text{NO}_2$ ratio (Fig. 6(a) and Fig. 6(b)).

419

420 Notably, the constant $\text{HONO}_{\text{corr}}/\text{NO}_2$ value at RH between 75-95% under the
421 condition of high $\text{PM}_{2.5}$ mass loading (Fig. 6(b)), compared to the downward trend of
422 $\text{HONO}_{\text{corr}}/\text{NO}_2$ within the same humidity range in low $\text{PM}_{2.5}$ mass concentration (Fig.
423 6(a)), implies a contribution of aerosol surfaces to the NO_2 -HONO conversion. Since

424 both $\text{HONO}_{\text{corr}}/\text{NO}_2$ in Fig. 6(a) and Fig. 6(b) are affected by the ground surfaces, we
425 can use the difference of $\text{HONO}_{\text{corr}}/\text{NO}_2$ between the two figures to represent the
426 influence of aerosol. As the area of shadow showed in Fig. 6(b), the aerosol-affected
427 $\text{HONO}_{\text{corr}}/\text{NO}_2$ is positively related to RH before RH reaches 95%. With the increase
428 of RH, the hygroscopic growth of aerosol particles should provide larger surface area.
429 When RH is higher than 75%, which has exceeded the mutual deliquescence relative
430 humidity of inorganic salts (Fountoukis and Nenes, 2007), aerosols will transfer to
431 aqueous phase gradually, and then promoting multiphase or heterogeneous chemistry
432 processes (Herrmann et al., 2015). For example, the oxidation of SO_2 by NO_2 on
433 aqueous aerosol surface may produce $\text{NO}_2^-/\text{HONO}$ efficiently under polluted
434 condition (Xie et al., 2015; Wang et al., 2016). In addition, the enhancement NO_2
435 uptake on micro-droplets by anions has been reported in experiments (Yabushita et al.,
436 2009)

437 438 **3.3.3. Impact of aerosols on HONO formation** 439

440 To further understand the heterogeneous formation of HONO on aerosol, we carry out
441 a correlation analysis when $\text{HONO}_{\text{corr}}/\text{NO}_2$ reaches the pseudo steady state at each
442 night (3:00-6:00 LT). The convergence or diffusion processes of gases and particles
443 caused by the decrease or increase of the boundary layer height can also lead to a
444 consistent trend of $\text{HONO}_{\text{corr}}$ and $\text{PM}_{2.5}$ (Fig. 7a), while the ratio of $\text{HONO}_{\text{corr}}$ and
445 NO_2 can not only reduce this physical effect but also represent the conversion degree
446 of NO_2 to HONO, so a moderate positive correlation between $\text{HONO}_{\text{corr}}/\text{NO}_2$ and
447 $\text{PM}_{2.5}$ ($r=0.35$, $p=0.01$) throughout the observation period could be more convincing
448 (Fig. 7b). As shown by larger triangles with gray borders in Fig. 7(b), $\text{HONO}_{\text{corr}}/\text{NO}_2$
449 is better correlated with $\text{PM}_{2.5}$ in the months when the mass concentrations of $\text{PM}_{2.5}$
450 are higher during this 1-year measurement, generally occurring from November to
451 May (Fig. 1d). This finding can be explained with a law that greater contributions of
452 NO_2 heterogeneously reacting on aerosol surface to HONO cause better correlations
453 between $\text{HONO}_{\text{corr}}/\text{NO}_2$ and $\text{PM}_{2.5}$. Interestingly, this relationship can also be divided
454 approximately into two groups by NH_3/CO ; the correlation is good when the value of

455 NH₃/CO is lower than 2‰, but when NH₃/CO is higher than 2‰, a poor correlation is
 456 found. We will discuss this phenomenon further in section 4. The evidence of HONO
 457 formation on aerosol were also found in other observations (Reisinger, 2000; Wang,
 458 2003; Li et al., 2012; Nie et al., 2015; Hou et al., 2016; Cui et al., 2018).

459

460 As is known, producing HONO is not the dominant sink of NO₂ at night, but it seems
 461 that more NO₂ can be converted to HONO under conditions of heavy pollution (Fig.
 462 7b). We discuss whether heterogeneous reactions of NO₂ on aerosols are able to
 463 provide comparable HONO with our measurement by Eq. (8), only considering
 464 HONO formation on particle surfaces and assuming that HONO principally settles on
 465 the ground surface, neglecting HONO loss on aerosol. c_{NO_2} is the mean molecular

466 velocity of NO₂ (370m/s); $[\frac{S}{V}]_{\text{aer}}$ is the surface area to volume ratio (m⁻¹) of aerosol;

467 v_{HONO} is the deposition velocity of HONO, which is considered to be close to the
 468 deposition velocity of NO₂ at night (Stutz et al., 2002; Su et al., 2008a); and a
 469 approximate value of 0.1cm/s is used based on the measurements from Coe and
 470 Gallagher (1992) and Stutz et al. (2002); H is the boundary layer mixing depth, and a
 471 value of 100m is assumed for nighttime (Su et al., 2008a).

472

$$473 \quad C_{\text{HONO}} = \frac{1}{4} \gamma_{\text{NO}_2 \rightarrow \text{HONO}} c_{\text{NO}_2} \left[\frac{S}{V} \right]_{\text{aer}} - \frac{v_{\text{HONO}}}{H} \frac{[\text{HONO}]}{[\text{NO}_2]} \quad (8)$$

474

475 Considering at nighttime period with severe haze in winter, the aerosol surface
 476 density calculated from the particle number size distributions between 6 nm and 800
 477 nm is about $1.2 \times 10^{-3} \text{ m}^{-1}$, matched by $200 \mu\text{g}/\text{m}^3$ of PM_{2.5} from our observations, and
 478 the averaged mixing ratios of HONO and NO₂ are 1.15 ppb and 28.4 ppb, respectively
 479 (Table 2). For 30%-100% of the measured mean C_{HONO} (0.0043 h^{-1}) in winter, the
 480 uptake coefficient of NO₂-to-HONO ($\gamma_{\text{NO}_2 \rightarrow \text{HONO}}$) calculated from Eq. (8) is in the range
 481 of 6.9×10^{-6} to 1.44×10^{-5} , consistent with the results from many laboratory studies

482 which demonstrate that the uptake coefficients of NO₂ (γ_{NO_2}) on multiple aerosol
483 surfaces or wet surfaces are mainly distributed around 10⁻⁵ with the HONO yield
484 varying from 0.1 to 0.9 (Grassian, 2002; Aubin and Abbatt, 2007; Khalizov et al.,
485 2010; Han et al., 2017). It is necessary to elaborate that: (1) the ambient particles were
486 dried with silica gel before measuring their number size distributions, and the mass
487 concentrations of PM_{2.5} were also measured under a system where the temperature
488 was maintained at 30°C, **usually above ambient temperature**; (2) the aerosol surface
489 was calculated by assuming that all particles are spherically shaped, but the particles
490 could in fact have irregular bodies and porous structure; (3) the particle size of both
491 PM_{2.5} and derived $[\frac{S}{V}]_{\text{aer}}$ is just a part of the total suspended particulate matter. As
492 described, the aerosol surface in the atmosphere is actually underestimated in our
493 study, thus the $\gamma_{\text{NO}_2 \rightarrow \text{HONO}}$ we derived could be the upper limit of the uptake coefficient
494 for NO₂ conversion to HONO on aerosol. In addition to particles surfaces, other
495 aerosol parameters such as surface water content, chemical composition, pH value,
496 and phase state of surfaces may also influence the heterogeneous formation of
497 HONO.

498

499 ***3.4. Missing daytime HONO source***

500

501 After discussing the nocturnal formation mechanism of HONO, we now focus on
502 the chemistry of daytime HONO **whose concentrations are still about 0.25-0.6 ppb at**
503 **noon with a lifetime of only 10-20 min** (Fig. 2). We are not certain if the observed
504 HONO can be provided by known mechanisms (gas phase reaction (R4) and
505 emissions) to date, so a budget equation of daytime HONO (Eq. 9) is utilized to
506 analyze its source and sinks (Su et al., 2008b; Sörgel et al., 2011). Here, dHONO/dt is
507 the change rate of the observed HONO. The sources rates of HONO contain the
508 homogeneous formation rate ($P_{\text{NO}+\text{OH}}$, R4); the combustion emission rate (P_{emis}); and
509 the unknown HONO daytime source (P_{unknown}). The sink rates of HONO consist of the
510 photolysis rate (L_{phot} , R1); the reaction rate of HONO with OH ($L_{\text{HONO}+\text{OH}}$, R2); and

511 the dry deposition rate (L_{dep}). T_v and T_h represent the vertical (T_v) and horizontal (T_h)
 512 transport processes of HONO, which are thought to be negligible for intense radiation
 513 and relatively homogeneous atmospheres with generally calm winds (Dillon, 2002; Su
 514 et al., 2008b; Sörgel et al., 2011).

515

$$516 \quad \frac{d\text{HONO}}{dt} = (P_{\text{NO+OH}} + P_{\text{emis}} + P_{\text{unknown}}) - (L_{\text{phot}} + L_{\text{HONO+OH}} + L_{\text{dep}}) + T_v + T_h \quad (9)$$

517

518 Therefore, the undiscovered daytime source of HONO (P_{unknown}) can be derived by Eq.
 519 (10), which is a deformation of Eq. (9) without minor terms (T_v and T_h) and where
 520 $d\text{HONO}/dt$ is substituted by $\Delta\text{HONO}/\Delta t$ that is counted as difference between
 521 observed HONO at two time points. The reaction rate constants of reaction 2
 522 ($k_{\text{HONO+OH}}$) and reaction 4 ($k_{\text{NO+OH}}$) are $6.0 \times 10^{-12} \text{ cm}^3 \text{ molecules}^{-1} \text{ s}^{-1}$ and 9.8×10^{-12}
 523 $\text{cm}^3 \text{ molecules}^{-1} \text{ s}^{-1}$, respectively (Atkinson et al., 2004). The emission ratio of
 524 HONO and NO_x ($\text{HONO}/\text{NO}_x = 0.79\%$) obtained in section 3.2, is used to estimate
 525 P_{emis} . For L_{dep} , the dry deposition velocity of diurnal HONO (v_{HONO}) is measured as 2
 526 cm/s in the work of Harrison et al. (1996), and a practical mixing height of 200 m is
 527 adopted, considering that most of the HONO cannot rise above this altitude due to
 528 rapid photolysis (Alicke et al., 2002).

529

$$530 \quad P_{\text{unknown}} = J(\text{HONO})[\text{HONO}] + k_{\text{HONO+OH}}[\text{HONO}][\text{OH}] + \frac{v_{\text{HONO}}}{H}[\text{HONO}] \quad (10)$$

$$+ \frac{\Delta\text{HONO}}{\Delta t} - k_{\text{NO+OH}}[\text{NO}][\text{OH}] - \frac{0.79\% \times \Delta\text{NO}_x}{\Delta t}$$

531

532 Fig. 8 shows the average daytime HONO budget from 8:00 LT to 16:00 LT during
 533 different seasons. The major loss route of HONO is photodecomposition (L_{phot}) with
 534 an average value of 1.48 ppb/h at noontime (10:00-14:00 LT) during this observation
 535 period, next to dry deposition (L_{dep}) whose mean value at the same time is 0.2 ppb/h,
 536 and by $L_{\text{HONO+OH}}$ which is less than 6% of that of L_{phot} . For the sources of HONO
 537 around noon, the average homogeneous reaction rate between NO and OH ($P_{\text{NO+OH}}$) is

538 0.71 ppb/h and P_{emis} just gives a tiny part of HONO at a rate of 0.02 ppb/h, meaning
539 that most of HONO comes from an unknown source whose average rate (P_{unknown}) is
540 1.02 ppb/h, contributing about 58% of the production of HONO. Comparing summer
541 data, the mean unknown daytime source strength of HONO in Nanjing is almost at the
542 upper-middle level of those reported in the existing literature: 0.22 ppb/h at a rural
543 site of New York state, USA (Zhou et al., 2002); 0.5 ppb/h in a forest near Jülich,
544 Germany (Kleffmann, 2005); 0.77 ppb/h in a polluted rural area of the Pearl River
545 Delta, China (Li et al., 2012); 0.98 ppb/h at an urban site in Xi'an, China (Huang et al.,
546 2017); 1.7 ppb/h in an urban area of Santiago, Chile (Elshorbany et al., 2009); 2.95
547 ppb/h in the urban atmosphere of Jinan, China (Li et al., 2018). In our study, the OH
548 production rate from the missing HONO accounts for about 78% of total $P_{\text{OH}}(\text{HONO})$
549 (Fig. S2), suggesting that the unconventional source of HONO is of significance to
550 atmospheric oxidation.

551

552 Hence, we perform a correlation analysis to explore the potential unknown daytime
553 mechanisms of HONO (Table 3). P_{unknown} is better correlated with $\text{NO}_2 \cdot \text{UVB}$ than
554 with NO_2 or UVB alone in spring and autumn ($p=0.05$), perhaps associated with the
555 photo-enhanced conversion from NO_2 to HONO (George et al., 2005; Stemmler et al.,
556 2006; Stemmler et al., 2007). The average value of P_{unknown} normalized by NO_2 is 0.1
557 h^{-1} , over 18 times greater than the nighttime conversion rate (0.0055 h^{-1}), also
558 implying that P_{unknown} cannot be explained by the nocturnal mechanism of
559 NO_2 -to-HONO. Assuming that the height of a well-mixed boundary layer around
560 noon remains constant for each day, $\text{UVB} \cdot \text{NO}_2$ and $\text{UVB} \cdot \text{NO}_2 \cdot \text{PM}_{2.5}$ could be
561 proxies for photo-induced heterogeneous reactions of NO_2 on ground and aerosol
562 surfaces, respectively. We do not have any solid evidence to identify which surfaces
563 (ground or aerosol) are more important to the hypothetical photo-heterogeneous
564 reaction of NO_2 based on the present analysis. For the same reason, the photolysis of
565 particulate nitrates (NO_3^-) as a source of HONO (Ye et al., 2016; Ye et al., 2017)
566 cannot be determined whether it is momentous in our study. The comparisons of
567 correlation coefficients showed above follow the method provided by Meng et al.

568 (1992).

569

570 Our study suggest that the missing source of HONO should be considered in the air
571 quality forecasting or regional models to characterize atmospheric oxidizing capacity
572 better, especially in warm seasons (spring and summer). Based on the measurement
573 (Fig. S3), the light-induced heterogeneous conversion of NO₂ to HONO on aerosol
574 surfaces and ground surface can been included in simulation works probably, as what
575 did in Lee et al. (2016).

576

577 *4. Semi-quantitative estimation of the contribution from different sources*

578

579 From this and previous studies, we can conclude that not only the concentration of
580 ambient HONO but also the sources of HONO have temporal and spatial patterns,
581 which is supposed to be considered in model studies. Nocturnal HONO is selected to
582 discuss the monthly variations of HONO sources in detail without the uncertainties of
583 daytime HONO formation, the influences of HONO photolysis, and the mixing effect
584 of boundary layer. The heterogeneous reaction of NO₂ on aerosol produces a
585 considerable portion of HONO in relatively polluted months (Dec.-May), but
586 contributes very little less than nothing in clean months (Jun.-Oct.), as seen in section
587 3.3.3. Coincidentally, direct emissions from burning processes of HONO decrease
588 from their peak values from winter to summer (section 3.2). However, the monthly
589 averaged ratios of HONO and NO_x are highest in summer, which conflicts with two
590 sources mentioned above.

591

592 As is known, higher NO₂-to-HONO conversion level or other NO_x-independent
593 sources can cause an increase in the HONO/NO_x ratio. For the case of a mostly
594 constant surface with low reactivity due to the long-term exposure to oxidizing gases
595 and radiation, the yield of nighttime HONO from NO₂ reacting on ground surfaces
596 could be imprecisely assumed to be unchanged. Thus, soil nitrite formed through
597 microbial activities, especially nitrification by ammonia-oxidizing bacteria
598 (NH₄⁺→NO₂⁻) (Su et al., 2011;Oswald et al., 2013), is adopted to be an source for

599 atmospheric HONO in this study, considering the nearby presence of some grassland
600 and natural vegetation mosaics. Although we do not directly measure HONO
601 emissions from soil, the observed ammonia can represent its monthly average
602 intensity, based on the following hypothesis: the dominant source of NH_3 is from soil,
603 especially from fertilizers ($\text{NH}_4^+ \rightarrow \text{NH}_3$) for a good correlation between ammonia and
604 temperature in the site ($r=0.63$, $p=0.01$), omitting the contributions of livestock to
605 NH_3 since there is only a small poultry facility within 10 km of this site (Meng et al.,
606 2011;Huang et al., 2012;Behera et al., 2013). Combustion sources (vehicles, industry,
607 biomass burning) should contribute only a fraction of NH_3 seeing that NH_3 is not
608 related to NO_x or CO in our study. Moreover, the release of both HONO and NH_3
609 depend on the strength of microbial activities, fertilizing amount, and soil properties
610 (e.g., temperature, acidity and water content of soil). Although the processes of
611 HONO and NH_3 emission from soil may not be completely synchronized, the
612 seasonal patterns for each should be consistent.

613

614 Until now, we can separate the sources of HONO into four parts: (1) combustion
615 emissions from vehicles and industries (HONO_{emi}) with a constant emitted
616 HONO/ NO_x ratio of 0.79%; (2) conversion of NO_2 to HONO on the ground surfaces
617 (HONO_{grd}) with a constant but unknown yield x_1 ; (3) conversion of NO_2 to HONO on
618 aerosol surfaces (HONO_{aer}) with a $\text{PM}_{2.5}$ -dependent yield ($\text{HONO}_{\text{aer}}/\text{NO}_2$); and (4)
619 emission from soil (HONO_{soi}), expressed by corrected NH_3 multiplied by an unknown
620 coefficient x_2 . The corrected NH_3 is obtained by subtracting combustion emission
621 from total observed ammonia. Ammonia from combustion is found to be proportional
622 to simultaneous CO (Meng et al., 2011;Chang et al., 2016), and a proportion of 0.3%,
623 which is in the lower quantile of the NH_3/CO ratios in fresh air masses (for hourly
624 data: $\text{NO}/\text{NO}_x > 0.75$; $\text{UVB} = 0$; temperature < 5 °C) is used from our measurements.
625 Substituting monthly average values of measured HONO, NO_2 , $\text{PM}_{2.5}$, NH_3 , and CO
626 into Eq.(11) by assuming that HONO_{tot} is equal to HONO_{obs} , we can get an
627 overdetermined system of equations, which have 11 equations with 2 unknowns
628 (excluding mean values of related parameters from February), and then we derive an

629 [approximate solution](#) ($x_1=1.89%$, $x_2=1.62%$) by the method of ordinary least squares.

630

631 Fig. 9 shows that an average of 36% of HONO is produced heterogeneously on
632 ground surfaces without perceptible temporal variations, but the contribution of this
633 source is overtaken by NO₂ converting to HONO on aerosols in January
634 (approximately 40% of HONO), and was exceeded by soil emission in July and
635 August (approximately 40% of HONO). The seasonal variations of HONO from
636 different pathways at night indicate that short-term observations may just capture a
637 small part of the total picture when exploring the source mechanisms of HONO. The
638 total HONO concentration (HONO_{tot}) is the sum of derived HONO from the four
639 sources listed above. The good correlation between HONO_{tot} and HONO_{obs} and the
640 low mean normalized error of HONO_{tot} to HONO_{obs} reveal that our assumption on
641 nocturnal HONO sources is reasonable. It should be noted that the slope of the
642 linearly fitted line between HONO_{corr}/NO₂ and PM_{2.5} in spring ($r=0.74$, slope=0.68‰)
643 is much higher than that in winter ($r=0.60$, slope=0.20‰), but we just use a mean
644 slope of 0.26‰ to evaluate aerosol effects throughout the year, this may be why our
645 method underestimates HONO in March and April and overestimates HONO in
646 January, and indicating that the mass concentration of PM_{2.5} is not the only factor
647 affecting formation of HONO on aerosols. Besides, lacking considerations of the
648 impact of RH and temperature on NO₂-to-HONO conversion and of seasonal
649 variations in ground surface properties, uncertainties of NO₂-to-HONO conversion
650 mechanisms and of combustion HONO emissions, and lacking direct observation for
651 soil emitted HONO, could all result in the bias between HONO_{tot} and HONO_{obs}, so
652 more studies on the detailed mechanism of various HONO sources need to be
653 performed.

654

$$\frac{[\text{HONO}_{\text{grd}}]}{[\text{NO}_2]} = X_1$$

$$\frac{[\text{HONO}_{\text{aer}}]}{[\text{NO}_2]} = 0.26\% \times [\text{PM}_{2.5}]$$

$$655 \quad \frac{[\text{HONO}_{\text{emi}}]}{[\text{NO}_x]} = 0.79\% \quad (11)$$

$$\frac{[\text{HONO}_{\text{soi}}]}{[\text{NH}_3] - 0.3\% \times [\text{CO}]} = X_2$$

$$\text{HONO}_{\text{tot}} = \text{HONO}_{\text{emi}} + \text{HONO}_{\text{soi}} + \text{HONO}_{\text{grd}} + \text{HONO}_{\text{aer}}$$

656

657 *5. Conclusions*

658

659 Continuous field measurement of HONO over 1 year was conducted at the SORPES
 660 station in Nanjing in the western YRD, China, from December 2017 to December
 661 2018. The observed seasonal average concentrations of HONO are in the range of
 662 0.45-1.04 ppb, which are comparable to those in other urban or suburban regions and
 663 appears to be of vital importance to atmospheric oxidation as the net OH production
 664 rate of HONO is about 1.5 times as that of ozone at daytime. HONO and NO_x have
 665 coincident monthly variations peaking in December and decreasing to the lowest
 666 value in August, and have similar diurnal pattern with the highest value in the early
 667 morning and a low point in the late afternoon, both indicating that NO_x is a crucial
 668 precursor of HONO.

669

670 Combustion emissions contribute an average of 23% to nocturnal HONO
 671 concentrations, with an average emission ratio $\Delta\text{HONO}/\Delta\text{NO}_x$ of 0.79%. During the
 672 nighttime, the dominant source of RH-dependent HONO could be the heterogeneous
 673 reaction of NO₂ on wet ground or aerosol surfaces with a mean estimated conversion
 674 rate of 0.0055 h⁻¹. During the daytime, a missing HONO source with an average
 675 strength of 1.02 ppb/h was identified around noon, contributing about 58% of the
 676 production of HONO and seeming to be photo-enhanced. HONO released from soil is
 677 adopted to discuss the seasonal changes of nocturnal HONO, and can contribute 40%
 678 to HONO during summer. Ground formation provides a major part of HONO at a

679 roughly constant proportion of 36%. The uptake of NO₂ on aerosol surface could
680 generate the greatest amount of HONO during heavily polluted periods (e.g. January).
681 Our results draw a complete picture of the sources of HONO during different seasons,
682 and demonstrated the needs of long-term and comprehensive observations to improve
683 the understanding of HONO chemistry.

684 **Author contribution**

685 W.N. and A.D. designed the study; Y.L. and W.N. wrote the manuscript; Y.L., Z.X.
686 and R.X. collected the HONO data and contributed to the data analysis; T.W., Y.L.,
687 L.W. and X.C. collected other related data, e.g. NH₃, NO_x and PM_{2.5}.

688 **Acknowledgments**

689 This work was mainly funded by the National Key R&D Program of China
690 (2016YFC0202000 and 2016YFC0200500), and the National Natural Science
691 Foundation of China (NSFC) project (D0512/41675145 and D0510/41605098). Data
692 analysis was also supported by other NSFC projects (D0512/41875175 and
693 D0510/41605098), Jiangsu Provincial Science Fund (BK20160620).

694 **References**

- 695
696 Acker, K., Febo, A., Trick, S., Perrino, C., Bruno, P., Wiesen, P., Möller, D., Wieprecht, W., Auel,
697 R., and Giusto, M.: Nitrous acid in the urban area of Rome, *Atmos. Environ.*, 40, 3123-3133,
698 2006.
- 699 Ackermann, R.: Auswirkungen von Kraftfahrzeugemissionen in der urbanen Atmosphäre,
700 Dissertation. de, 2000.
- 701 Alicke, B.: Impact of nitrous acid photolysis on the total hydroxyl radical budget during the
702 Limitation of Oxidant Production/Pianura Padana Produzione di Ozono study in Milan, *Journal of*
703 *Geophysical Research*, 107, 10.1029/2000jd000075, 2002.
- 704 Alicke, B., Platt, U., and Stutz, J.: Impact of nitrous acid photolysis on the total hydroxyl radical
705 budget during the Limitation of Oxidant Production/Pianura Padana Produzione di Ozono study in
706 Milan, *Journal of Geophysical Research: Atmospheres*, 107, LOP 9-1-LOP 9-17, 2002.
- 707 Alicke, B.: OH formation by HONO photolysis during the BERLIOZ experiment, *Journal of*
708 *Geophysical Research*, 108, 10.1029/2001jd000579, 2003.
- 709 Ammann, M., Kalberer, M., Jost, D., Tobler, L., Rössler, E., Piguet, D., Gaggeler, H., and
710 Baltensperger, U.: Heterogeneous production of nitrous acid on soot in polluted air masses,

711 NATURE, 395, 157-160, 10.1038/25965, 1998.

712 Ammann, M., Rossler, E., Strekowski, R., and George, C.: Nitrogen dioxide multiphase chemistry:
713 uptake kinetics on aqueous solutions containing phenolic compounds, *Phys Chem Chem Phys*, 7,
714 2513-2518, 10.1039/b501808k, 2005.

715 Atkinson, R.: Atmospheric chemistry of VOCs and NO_x, *Atmos. Environ.*, 34, 2063-2101, 2000.

716 Atkinson, R., Baulch, D., Cox, R., Crowley, J., Hampson, R., Hynes, R., Jenkin, M., Rossi, M.,
717 and Troe, J.: Evaluated kinetic and photochemical data for atmospheric chemistry: Volume I-gas
718 phase reactions of O_x, HO_x, NO_x and SO_x species, *Atmospheric chemistry and physics*, 4,
719 1461-1738, 2004.

720 Aubin, D. G., and Abbatt, J. P.: Interaction of NO₂ with hydrocarbon soot: Focus on HONO yield,
721 surface modification, and mechanism, *The Journal of Physical Chemistry A*, 111, 6263-6273,
722 2007.

723 Behera, S. N., Sharma, M., Aneja, V. P., and Balasubramanian, R.: Ammonia in the atmosphere: a
724 review on emission sources, atmospheric chemistry and deposition on terrestrial bodies, *Environ*
725 *Sci Pollut Res Int*, 20, 8092-8131, 10.1007/s11356-013-2051-9, 2013.

726 Bernard, F., Cazaunau, M., Grosselin, B., Zhou, B., Zheng, J., Liang, P., Zhang, Y., Ye, X., Daele,
727 V., Mu, Y., Zhang, R., Chen, J., and Mellouki, A.: Measurements of nitrous acid (HONO) in
728 urban area of Shanghai, China, *Environ Sci Pollut Res Int*, 23, 5818-5829,
729 10.1007/s11356-015-5797-4, 2016.

730 Canfield, D. E., Glazer, A. N., and Falkowski, P. G.: The Evolution and Future of Earth's
731 Nitrogen Cycle, *Science*, 330, 192-196, 10.1126/science.1186120, 2010.

732 Chang, Y., Zou, Z., Deng, C., Huang, K., Collett, J. L., Lin, J., and Zhuang, G.: The importance of
733 vehicle emissions as a source of atmospheric ammonia in the megacity of Shanghai, *Atmospheric*
734 *Chemistry and Physics*, 16, 3577, 2016.

735 Coe, H., and Gallagher, M.: Measurements of dry deposition of NO₂ to a Dutch heathland using
736 the eddy-correlation technique, *Quarterly Journal of the Royal Meteorological Society*, 118,
737 767-786, 1992.

738 Cui, L., Li, R., Zhang, Y., Meng, Y., Fu, H., and Chen, J.: An observational study of nitrous acid
739 (HONO) in Shanghai, China: The aerosol impact on HONO formation during the haze episodes,
740 *Sci Total Environ*, 630, 1057-1070, 10.1016/j.scitotenv.2018.02.063, 2018.

741 Dillon, M. B.: Chemical evolution of the Sacramento urban plume: Transport and oxidation, 2002.

742 Ding, A., Nie, W., Huang, X., Chi, X., Sun, J., Kerminen, V.-M., Xu, Z., Guo, W., Petäjä, T.,
743 Yang, X., Kulmala, M., and Fu, C.: Long-term observation of air pollution-weather/climate
744 interactions at the SORPES station: a review and outlook, *Frontiers of Environmental Science &*
745 *Engineering*, 10, 10.1007/s11783-016-0877-3, 2016.

746 Ding, A. J., Fu, C. B., Yang, X. Q., Sun, J. N., Zheng, L. F., Xie, Y. N., Herrmann, E., Nie, W.,
747 Petäjä, T., Kerminen, V. M., and Kulmala, M.: Ozone and fine particle in the western Yangtze
748 River Delta: an overview of 1 yr data at the SORPES station, *Atmospheric Chemistry and Physics*,
749 13, 5813-5830, 10.5194/acp-13-5813-2013, 2013.

750 Dusanter, S., Vimal, D., Stevens, P., Volkamer, R., and Molina, L.: Measurements of OH and
751 HO₂ concentrations during the MCMA-2006 field campaign—Part 1: Deployment of the Indiana
752 University laser-induced fluorescence instrument, *Atmospheric Chemistry and Physics*, 9,
753 1665-1685, 2009.

754 Elshorbany, Y. F., Kurtenbach, R., Wiesen, P., Lissi, E., Rubio, M., Villena, G., Gramsch, E.,

755 Rickard, A., Pilling, M., and Kleffmann, J.: Oxidation capacity of the city air of Santiago, Chile,
756 Atmospheric Chemistry and Physics, 9, 2257-2273, 2009.

757 Finlayson-Pitts, B. J., and Pitts, J. N.: CHAPTER 6 - Rates and Mechanisms of Gas-Phase
758 Reactions in Irradiated Organic – NO_x – Air Mixtures, in: Chemistry of the Upper and Lower
759 Atmosphere, edited by: Finlayson-Pitts, B. J., and Pitts, J. N., Academic Press, San Diego,
760 179-263, 2000.

761 Finlayson-Pitts, B. J., Wingen, L. M., Sumner, A. L., Syomin, D., and Ramazan, K. A.: The
762 heterogeneous hydrolysis of NO₂ in laboratory systems and in outdoor and indoor atmospheres:
763 An integrated mechanism, Physical Chemistry Chemical Physics, 5, 223-242, 10.1039/b208564j,
764 2003.

765 Fountoukis, C., and Nenes, A.: ISORROPIA II: a computationally efficient thermodynamic
766 equilibrium model for K⁺-Ca²⁺-Mg²⁺-NH₄⁽⁺⁾-Na⁺-SO₄²⁻-NO₃⁻-Cl⁻-H₂O aerosols,
767 Atmospheric Chemistry and Physics, 7, 4639-4659, 10.5194/acp-7-4639-2007, 2007.

768 George, C., Streckowski, R. S., Kleffmann, J., Stemmler, K., and Ammann, M.: Photoenhanced
769 uptake of gaseous NO₂ on solid organic compounds: a photochemical source of HONO?, Faraday
770 Discussions, 130, 195, 10.1039/b417888m, 2005.

771 Grassian, V.: Chemical reactions of nitrogen oxides on the surface of oxide, carbonate, soot, and
772 mineral dust particles: Implications for the chemical balance of the troposphere, The Journal of
773 Physical Chemistry A, 106, 860-877, 2002.

774 Han, C., Liu, Y., and He, H.: Heterogeneous reaction of NO₂ with soot at different relative
775 humidity, Environmental Science and Pollution Research, 24, 21248-21255,
776 10.1007/s11356-017-9766-y, 2017.

777 Hao, N., Zhou, B., Chen, D., and Chen, L.-m.: Observations of nitrous acid and its relative
778 humidity dependence in Shanghai, Journal of Environmental Sciences, 18, 910-915,
779 10.1016/s1001-0742(06)60013-2, 2006.

780 Harrison, R. M., Peak, J. D., and Collins, G. M.: Tropospheric cycle of nitrous acid, Journal of
781 Geophysical Research: Atmospheres, 101, 14429-14439, 1996.

782 Heland, J., Kleffmann, J., Kurtenbach, R., and Wiesen, P.: A new instrument to measure
783 gaseous nitrous acid (HONO) in the atmosphere, Environmental Science & Technology, 35,
784 3207-3212, 2001.

785 Hendrick, F., Müller, J. F., Clémer, K., Wang, P., De Mazière, M., Fayt, C., Gielen, C., Hermans,
786 C., Ma, J. Z., Pinardi, G., Stavrou, T., Vlemmix, T., and Van Roozendaal, M.: Four years of
787 ground-based MAX-DOAS observations of HONO and NO₂ in the
788 Beijing area, Atmospheric Chemistry and Physics, 14, 765-781, 10.5194/acp-14-765-2014, 2014.

789 Herrmann, H., Schaefer, T., Tilgner, A., Styler, S. A., Weller, C., Teich, M., and Otto, T.:
790 Tropospheric aqueous-phase chemistry: kinetics, mechanisms, and its coupling to a changing gas
791 phase, Chem Rev, 115, 4259-4334, 10.1021/cr500447k, 2015.

792 Hou, S., Tong, S., Ge, M., and An, J.: Comparison of atmospheric nitrous acid during severe haze
793 and clean periods in Beijing, China, Atmos. Environ., 124, 199-206,
794 10.1016/j.atmosenv.2015.06.023, 2016.

795 Huang, R. J., Yang, L., Cao, J., Wang, Q., Tie, X., Ho, K. F., Shen, Z., Zhang, R., Li, G., Zhu, C.,
796 Zhang, N., Dai, W., Zhou, J., Liu, S., Chen, Y., Chen, J., and O'Dowd, C. D.: Concentration and
797 sources of atmospheric nitrous acid (HONO) at an urban site in Western China, Sci Total Environ,
798 593-594, 165-172, 10.1016/j.scitotenv.2017.02.166, 2017.

799 Huang, X., Song, Y., Li, M., Li, J., Huo, Q., Cai, X., Zhu, T., Hu, M., and Zhang, H.: A
800 high-resolution ammonia emission inventory in China, *Global Biogeochemical Cycles*, 26, n/a-n/a,
801 10.1029/2011gb004161, 2012.

802 Jarvis, D. L., Leaderer, B. P., Chinn, S., and Burney, P. G.: Indoor nitrous acid and respiratory
803 symptoms and lung function in adults, *Thorax*, 60, 474-479, 10.1136/thx.2004.032177, 2005.

804 Jenkin, M. E., Cox, R. A., and Williams, D. J.: Laboratory studies of the kinetics of formation of
805 nitrous acid from the thermal reaction of nitrogen dioxide and water vapour, *Atmos. Environ.*, 22,
806 487-498, 1988.

807 Kalberer, M., Ammann, M., Arens, F., Gäggeler, H. W., and Baltensperger, U.: Heterogeneous
808 formation of nitrous acid (HONO) on soot aerosol particles, *Journal of Geophysical Research:*
809 *Atmospheres*, 104, 13825-13832, 10.1029/1999jd900141, 1999.

810 Kanaya, Y., Cao, R., Akimoto, H., Fukuda, M., Komazaki, Y., Yokouchi, Y., Koike, M.,
811 Tanimoto, H., Takegawa, N., and Kondo, Y.: Urban photochemistry in central Tokyo: 1. Observed
812 and modeled OH and HO₂ radical concentrations during the winter and summer of 2004, *Journal*
813 *of Geophysical Research*, 112, 10.1029/2007jd008670, 2007.

814 Khalizov, A. F., Cruz-Quinones, M., and Zhang, R.: Heterogeneous reaction of NO₂ on fresh and
815 coated soot surfaces, *The Journal of Physical Chemistry A*, 114, 7516-7524, 2010.

816 Kirchner, U., Scheer, V., and Vogt, R.: FTIR spectroscopic investigation of the mechanism and
817 kinetics of the heterogeneous reactions of NO₂ and HNO₃ with soot, *The Journal of Physical*
818 *Chemistry A*, 104, 8908-8915, 2000.

819 Kirchstetter, T., Harley, R., and Littlejohn, D.: Measurement of Nitrous Acid in Motor Vehicle
820 Exhaust, *Environmental Science & Technology Letters*, 30, 2843-2849, 10.1021/es960135y, 1996.

821 Kleffmann, J., Becker, K., and Wiesen, P.: Heterogeneous NO₂ conversion processes on acid
822 surfaces: Possible atmospheric implications, *Atmos. Environ.*, 32, 2721-2729,
823 10.1016/S1352-2310(98)00065-X, 1998.

824 Kleffmann, J., Becker, K. H., Lackhoff, M., and Wiesen, P.: Heterogeneous conversion of NO₂ on
825 carbonaceous surfaces, *Physical Chemistry Chemical Physics*, 1, 5443-5450, 1999.

826 Kleffmann, J.: Daytime formation of nitrous acid: A major source of OH radicals in a forest,
827 *Geophysical Research Letters*, 32, 10.1029/2005gl022524, 2005.

828 Kleffmann, J., Lörzer, J. C., Wiesen, P., Kern, C., Trick, S., Volkamer, R., Rodenas, M., and
829 Wirtz, K.: Intercomparison of the DOAS and LOPAP techniques for the detection of nitrous acid
830 (HONO), *Atmos. Environ.*, 40, 3640-3652, 10.1016/j.atmosenv.2006.03.027, 2006.

831 Kurtenbach, R., Becker, K., Gomes, J., Kleffmann, J., Lorzer, J., Spittler, M., Wiesen, P.,
832 Ackermann, R., Geyer, A., and Platt, U.: Investigations of emissions and heterogeneous formation
833 of HONO in a road traffic tunnel, *Atmos. Environ.*, 35, 3385-3394,
834 10.1016/S1352-2310(01)00138-8, 2001.

835 Lammel, G., and Cape, J. N.: Nitrous Acid and Nitrite in the Atmosphere, *CHEMICAL SOCIETY*
836 *REVIEWS*, 25, 361-369, 10.1039/cs9962500361, 1996.

837 Lammel, G.: Formation of nitrous acid: parameterisation and comparison with observations,
838 *Max-Planck-Institut für Meteorologie*, 1999.

839 Lee, J. D., Whalley, L. K., Heard, D. E., Stone, D., Dunmore, R. E., Hamilton, J. F., Young, D. E.,
840 Allan, J. D., Laufs, S., and Kleffmann, J.: Detailed budget analysis of HONO in central London
841 reveals a missing daytime source, *Atmospheric Chemistry and Physics*, 16, 2747-2764,
842 10.5194/acp-16-2747-2016, 2016.

843 Li, D., Xue, L., Wen, L., Wang, X., Chen, T., Mellouki, A., Chen, J., and Wang, W.:
844 Characteristics and sources of nitrous acid in an urban atmosphere of northern China: Results from
845 1-yr continuous observations, *Atmos. Environ.*, 182, 296-306, 10.1016/j.atmosenv.2018.03.033,
846 2018.

847 Li, X., Brauers, T., Häseler, R., Bohn, B., Fuchs, H., Hofzumahaus, A., Holland, F., Lou, S., Lu, K.
848 D., Rohrer, F., Hu, M., Zeng, L. M., Zhang, Y. H., Garland, R. M., Su, H., Nowak, A.,
849 Wiedensohler, A., Takegawa, N., Shao, M., and Wahner, A.: Exploring the atmospheric chemistry
850 of nitrous acid (HONO) at a rural site in Southern China, *Atmospheric Chemistry and Physics*, 12,
851 1497-1513, 10.5194/acp-12-1497-2012, 2012.

852 Lu, K. D., Rohrer, F., Holland, F., Fuchs, H., Bohn, B., Brauers, T., Chang, C. C., Haseler, R., Hu,
853 M., Kita, K., Kondo, Y., Li, X., Lou, S. R., Nehr, S., Shao, M., Zeng, L. M., Wahner, A., Zhang,
854 Y. H., and Hofzumahaus, A.: Observation and modelling of OH and HO₂ concentrations in the
855 Pearl River Delta 2006: a missing OH source in a VOC rich atmosphere, *Atmospheric Chemistry
856 and Physics*, 12, 1541-1569, 10.5194/acp-12-1541-2012, 2012.

857 Lu, K. D., Hofzumahaus, A., Holland, F., Bohn, B., Brauers, T., Fuchs, H., Hu, M., Haseler, R.,
858 Kita, K., Kondo, Y., Li, X., Lou, S. R., Oebel, A., Shao, M., Zeng, L. M., Wahner, A., Zhu, T.,
859 Zhang, Y. H., and Rohrer, F.: Missing OH source in a suburban environment near Beijing:
860 observed and modelled OH and HO₂ concentrations in summer 2006, *Atmospheric Chemistry and
861 Physics*, 13, 1057-1080, 10.5194/acp-13-1057-2013, 2013.

862 Lu, K. D., Rohrer, F., Holland, F., Fuchs, H., Brauers, T., Oebel, A., Dlugi, R., Hu, M., Li, X.,
863 Lou, S. R., Shao, M., Zhu, T., Wahner, A., Zhang, Y. H., and Hofzumahaus, A.: Nighttime
864 observation and chemistry of HO_x in the Pearl River Delta and Beijing in summer 2006,
865 *Atmospheric Chemistry and Physics*, 14, 4979-4999, 10.5194/acp-14-4979-2014, 2014.

866 Meng, X.-L., Rosenthal, R., and Rubin, D. B.: Comparing correlated correlation coefficients,
867 *Psychological bulletin*, 111, 172, 1992.

868 Meng, Z., Lin, W., Jiang, X., Yan, P., Wang, Y., Zhang, Y., Jia, X., and Yu, X.: Characteristics of
869 atmospheric ammonia over Beijing, China, *Atmospheric Chemistry and Physics*, 11, 6139-6151,
870 2011.

871 Meusel, H., Kuhn, U., Reiffs, A., Mallik, C., Harder, H., Martinez, M., Schuladen, J., Bohn, B.,
872 Parchatka, U., Crowley, J. N., Fischer, H., Tomsche, L., Novelli, A., Hoffmann, T., Janssen, R. H.
873 H., Hartogensis, O., Pikridas, M., Vrekoussis, M., Bourtsoukidis, E., Weber, B., Lelieveld, J.,
874 Williams, J., Pöschl, U., Cheng, Y., and Su, H.: Daytime formation of nitrous acid at a coastal
875 remote site in Cyprus indicating a common ground source of atmospheric HONO and NO,
876 *Atmospheric Chemistry and Physics*, 16, 14475-14493, 10.5194/acp-16-14475-2016, 2016.

877 Michoud, V., Colomb, A., Borbon, A., Miet, K., Beekmann, M., Camredon, M., Aumont, B.,
878 Perrier, S., Zapf, P., Siour, G., Ait-Helal, W., Afif, C., Kukui, A., Furger, M., Dupont, J. C.,
879 Haefelin, M., and Doussin, J. F.: Study of the unknown HONO daytime source at a European
880 suburban site during the MEGAPOLI summer and winter field campaigns, *Atmospheric
881 Chemistry and Physics*, 14, 2805-2822, 10.5194/acp-14-2805-2014, 2014.

882 Nie, W., Ding, A. J., Xie, Y. N., Xu, Z., Mao, H., Kerminen, V. M., Zheng, L. F., Qi, X. M.,
883 Huang, X., Yang, X. Q., Sun, J. N., Herrmann, E., Petäjä, T., Kulmala, M., and Fu, C. B.:
884 Influence of biomass burning plumes on HONO chemistry in eastern China, *Atmospheric
885 Chemistry and Physics*, 15, 1147-1159, 10.5194/acp-15-1147-2015, 2015.

886 Oswald, R., Behrendt, T., Ermel, M., Wu, D., Su, H., Cheng, Y., Breuninger, C., Moravek, A.,

887 Mougin, E., and Delon, C.: HONO emissions from soil bacteria as a major source of atmospheric
888 reactive nitrogen, *Science*, 341, 1233-1235, 2013.

889 Pagsberg, P., Bjergbakke, E., Ratajczak, E., and Sillesen, A.: Kinetics of the gas phase reaction
890 $\text{OH} + \text{NO} (+ \text{M}) \rightarrow \text{HONO} (+ \text{M})$ and the determination of the UV absorption cross sections of
891 HONO, *Chemical physics letters*, 272, 383-390, 1997.

892 Perner, D., and Platt, U.: Detection of nitrous acid in the atmosphere by differential optical
893 absorption, *Geophysical Research Letters*, 6, 917-920, doi:10.1029/GL006i012p00917, 1979.

894 Platt, U., Perner, D., Harris, G. W., Winer, A. M., and Pitts, J. N.: Observations of nitrous acid in
895 an urban atmosphere by differential optical absorption, *Nature*, 285, 312-314, 10.1038/285312a0,
896 1980.

897 Qi, X. M., Ding, A. J., Nie, W., Petäjä, T., Kerminen, V. M., Herrmann, E., Xie, Y. N., Zheng, L.
898 F., Manninen, H., Aalto, P., Sun, J. N., Xu, Z. N., Chi, X. G., Huang, X., Boy, M., Virkkula, A.,
899 Yang, X. Q., Fu, C. B., and Kulmala, M.: Aerosol size distribution and new particle formation in
900 the western Yangtze River Delta of China: 2 years of measurements at the SORPES station,
901 *Atmospheric Chemistry and Physics*, 15, 12445-12464, 10.5194/acp-15-12445-2015, 2015.

902 Rappenglück, B., Lubertino, G., Alvarez, S., Golovko, J., Czader, B., and Ackermann, L.: Radical
903 precursors and related species from traffic as observed and modeled at an urban highway junction,
904 *Journal of the Air & Waste Management Association*, 63, 1270-1286,
905 10.1080/10962247.2013.822438, 2013.

906 Reisinger, A. R.: Observations of HNO₂ in the polluted winter atmosphere: possible
907 heterogeneous production on aerosols, *Atmos. Environ.*, 34, 3865-3874, 2000.

908 Richter, A., Burrows, J. P., Nuss, H., Granier, C., and Niemeier, U.: Increase in tropospheric
909 nitrogen dioxide over China observed from space, *Nature*, 437, 129-132, 10.1038/nature04092,
910 2005.

911 Rohde, R. A., and Muller, R. A.: Air Pollution in China: Mapping of Concentrations and Sources,
912 *PLoS One*, 10, e0135749, 10.1371/journal.pone.0135749, 2015.

913 Rohrer, F., and Berresheim, H.: Strong correlation between levels of tropospheric hydroxyl
914 radicals and solar ultraviolet radiation, *Nature*, 442, 184-187, 10.1038/nature04924, 2006.

915 Saliba, N., Yang, H., and Finlayson-Pitts, B.: Reaction of gaseous nitric oxide with nitric acid on
916 silica surfaces in the presence of water at room temperature, *The Journal of Physical Chemistry A*,
917 105, 10339-10346, 2001.

918 Seinfeld, J. H., and Pandis, S. N.: *Atmospheric chemistry and physics: from air pollution to*
919 *climate change*, John Wiley & Sons, 2016.

920 Shao, P., Xin, J., An, J., Kong, L., Wang, B., Wang, J., Wang, Y., and Wu, D.: The empirical
921 relationship between PM_{2.5} and AOD in Nanjing of the Yangtze River Delta, *Atmospheric*
922 *Pollution Research*, 8, 233-243, 10.1016/j.apr.2016.09.001, 2017.

923 Shen, Y., Virkkula, A., Ding, A., Wang, J., Chi, X., Nie, W., Qi, X., Huang, X., Liu, Q., Zheng, L.,
924 Xu, Z., Petäjä, T., Aalto, P. P., Fu, C., and Kulmala, M.: Aerosol optical properties at SORPES in
925 Nanjing, east China, *Atmospheric Chemistry and Physics*, 18, 5265-5292,
926 10.5194/acp-18-5265-2018, 2018.

927 Sleiman, M., Gundel, L. A., Pankow, J. F., Jacob, P., 3rd, Singer, B. C., and Destailats, H.:
928 Formation of carcinogens indoors by surface-mediated reactions of nicotine with nitrous acid,
929 leading to potential thirdhand smoke hazards, *Proc Natl Acad Sci U S A*, 107, 6576-6581,
930 10.1073/pnas.0912820107, 2010.

931 Sörgel, M., Regelin, E., Bozem, H., Diesch, J. M., Drewnick, F., Fischer, H., Harder, H., Held, A.,
932 Hosaynali-Beygi, Z., Martinez, M., and Zetzsch, C.: Quantification of the unknown HONO
933 daytime source and its relation to NO₂, *Atmospheric Chemistry and Physics*, 11, 10433-10447,
934 10.5194/acp-11-10433-2011, 2011.

935 Stemmler, K., Ammann, M., Donders, C., Kleffmann, J., and George, C.: Photosensitized
936 reduction of nitrogen dioxide on humic acid as a source of nitrous acid, *Nature*, 440, 195-198,
937 10.1038/nature04603, 2006.

938 Stemmler, K., Ndour, M., Elshorbany, Y., Kleffmann, J., D'anna, B., George, C., Bohn, B., and
939 Ammann, M.: Light induced conversion of nitrogen dioxide into nitrous acid on submicron humic
940 acid aerosol, *Atmospheric Chemistry and Physics*, 7, 4237-4248, 2007.

941 Stutz, J., Kim, E. S., Platt, U., Bruno, P., Perrino, C., and Febo, A.: UV-visible absorption cross
942 sections of nitrous acid, *Journal of Geophysical Research: Atmospheres*, 105, 14585-14592,
943 10.1029/2000jd900003, 2000.

944 Stutz, J., Alicke, B., and Neftel, A.: Nitrous acid formation in the urban atmosphere: Gradient
945 measurements of NO₂ and HONO over grass in Milan, Italy, *Journal of Geophysical Research*,
946 107, 10.1029/2001jd000390, 2002.

947 Stutz, J., Alicke, B., Ackermann, R., Geyer, A., Wang, S., White, A. B., Williams, E. J., Spicer, C.
948 W., and Fast, J. D.: Relative humidity dependence of HONO chemistry in urban areas, *Journal of*
949 *Geophysical Research: Atmospheres*, 109, n/a-n/a, 10.1029/2003jd004135, 2004.

950 Su, H., Cheng, Y. F., Cheng, P., Zhang, Y. H., Dong, S., Zeng, L. M., Wang, X., Slanina, J., Shao,
951 M., and Wiedensohler, A.: Observation of nighttime nitrous acid (HONO) formation at a
952 non-urban site during PRIDE-PRD2004 in China, *Atmos. Environ.*, 42, 6219-6232,
953 10.1016/j.atmosenv.2008.04.006, 2008a.

954 Su, H., Cheng, Y. F., Shao, M., Gao, D. F., Yu, Z. Y., Zeng, L. M., Slanina, J., Zhang, Y. H., and
955 Wiedensohler, A.: Nitrous acid (HONO) and its daytime sources at a rural site during the 2004
956 PRIDE-PRD experiment in China, *Journal of Geophysical Research*, 113, 10.1029/2007jd009060,
957 2008b.

958 Su, H., Cheng, Y., Oswald, R., Behrendt, T., Trebs, I., Meixner, F. X., Andreae, M. O., Cheng, P.,
959 Zhang, Y., and Pöschl, U.: Soil nitrite as a source of atmospheric HONO and OH radicals, *Science*,
960 333, 1616-1618, 2011.

961 Sumner, A. L., Menke, E. J., Dubowski, Y., Newberg, J. T., Penner, R. M., Hemminger, J. C.,
962 Wingen, L. M., Brauers, T., and Finlayson-Pitts, B. J.: The nature of water on surfaces of
963 laboratory systems and implications for heterogeneous chemistry in the troposphere, *Physical*
964 *Chemistry Chemical Physics*, 6, 10.1039/b308125g, 2004.

965 Sun, P., Nie, W., Chi, X., Xie, Y., Huang, X., Xu, Z., Qi, X., Xu, Z., Wang, L., Wang, T., Zhang,
966 Q., and Ding, A.: Two years of online measurement of fine particulate nitrate in the western
967 Yangtze River Delta: influences of thermodynamics and
968 N_2O_5 hydrolysis, *Atmospheric Chemistry and*
969 *Physics*, 18, 17177-17190, 10.5194/acp-18-17177-2018, 2018.

970 Tong, S., Hou, S., Zhang, Y., Chu, B., Liu, Y., He, H., Zhao, P., and Ge, M.: Comparisons of
971 measured nitrous acid (HONO) concentrations in a pollution period at urban and suburban Beijing,
972 in autumn of 2014, *Science China Chemistry*, 58, 1393-1402, 10.1007/s11426-015-5454-2, 2015.

973 Underwood, G., Song, C., Phadnis, M., Carmichael, G., and Grassian, V.: Heterogeneous
974 reactions of NO₂ and HNO₃ on oxides and mineral dust: A combined laboratory and modeling

975 study, *Journal of Geophysical Research: Atmospheres*, 106, 18055-18066, 2001.

976 VandenBoer, T., Markovic, M., Sanders, J., Ren, X., Pusede, S., Browne, E., Cohen, R., Zhang, L.,
977 Thomas, J., and Brune, W.: Evidence for a nitrous acid (HONO) reservoir at the ground surface in
978 Bakersfield, CA, during CalNex 2010, *Journal of Geophysical Research: Atmospheres*, 119,
979 9093-9106, 2014a.

980 VandenBoer, T. C., Young, C. J., Talukdar, R. K., Markovic, M. Z., Brown, S. S., Roberts, J. M.,
981 and Murphy, J. G.: Nocturnal loss and daytime source of nitrous acid through reactive uptake and
982 displacement, *Nature Geoscience*, 8, 55-60, 10.1038/ngeo2298, 2014b.

983 Villena, G., Kleffmann, J., Kurtenbach, R., Wiesen, P., Lissi, E., Rubio, M. A., Croxatto, G., and
984 Rappenglück, B.: Vertical gradients of HONO, NO_x and O₃ in Santiago de Chile, *Atmos.*
985 *Environ.*, 45, 3867-3873, 10.1016/j.atmosenv.2011.01.073, 2011a.

986 Villena, G., Wiesen, P., Cantrell, C. A., Flocke, F., Fried, A., Hall, S. R., Hornbrook, R. S., Knapp,
987 D., Kosciuch, E., Mauldin, R. L., McGrath, J. A., Montzka, D., Richter, D., Ullmann, K., Walega,
988 J., Weibring, P., Weinheimer, A., Staebler, R. M., Liao, J., Huey, L. G., and Kleffmann, J.:
989 Nitrous acid (HONO) during polar spring in Barrow, Alaska: A net source of OH radicals?,
990 *Journal of Geophysical Research*, 116, 10.1029/2011jd016643, 2011b.

991 Wang, G., Zhang, R., Gomez, M. E., Yang, L., Levy Zamora, M., Hu, M., Lin, Y., Peng, J., Guo,
992 S., Meng, J., Li, J., Cheng, C., Hu, T., Ren, Y., Wang, Y., Gao, J., Cao, J., An, Z., Zhou, W., Li,
993 G., Wang, J., Tian, P., Marrero-Ortiz, W., Secrest, J., Du, Z., Zheng, J., Shang, D., Zeng, L., Shao,
994 M., Wang, W., Huang, Y., Wang, Y., Zhu, Y., Li, Y., Hu, J., Pan, B., Cai, L., Cheng, Y., Ji, Y.,
995 Zhang, F., Rosenfeld, D., Liss, P. S., Duce, R. A., Kolb, C. E., and Molina, M. J.: Persistent
996 sulfate formation from London Fog to Chinese haze, *Proc Natl Acad Sci U S A*, 113,
997 13630-13635, 10.1073/pnas.1616540113, 2016.

998 Wang, J., Zhang, X., Guo, J., Wang, Z., and Zhang, M.: Observation of nitrous acid (HONO) in
999 Beijing, China: Seasonal variation, nocturnal formation and daytime budget, *Sci Total Environ*,
1000 587-588, 350-359, 10.1016/j.scitotenv.2017.02.159, 2017.

1001 Wang, S.: Atmospheric observations of enhanced NO₂-HONO conversion on mineral dust
1002 particles, *Geophysical Research Letters*, 30, 10.1029/2003gl017014, 2003.

1003 Wang, S., Zhou, R., Zhao, H., Wang, Z., Chen, L., and Zhou, B.: Long-term observation of
1004 atmospheric nitrous acid (HONO) and its implication to local NO₂ levels in Shanghai, China,
1005 *Atmos. Environ.*, 77, 718-724, 10.1016/j.atmosenv.2013.05.071, 2013.

1006 Wentzell, J. J. B., Schiller, C. L., and Harris, G. W.: Measurements of HONO during BAQS-Met,
1007 *Atmospheric Chemistry and Physics*, 10, 12285-12293, 10.5194/acp-10-12285-2010, 2010.

1008 Wong, K. W., Oh, H. J., Lefer, B. L., Rappenglück, B., and Stutz, J.: Vertical profiles of nitrous
1009 acid in the nocturnal urban atmosphere of Houston, TX, *Atmospheric Chemistry and Physics*, 11,
1010 3595-3609, 10.5194/acp-11-3595-2011, 2011.

1011 Xie, Y., Ding, A., Nie, W., Mao, H., Qi, X., Huang, X., Xu, Z., Kerminen, V.-M., Petäjä, T., Chi,
1012 X., Virkkula, A., Boy, M., Xue, L., Guo, J., Sun, J., Yang, X., Kulmala, M., and Fu, C.: Enhanced
1013 sulfate formation by nitrogen dioxide: Implications from in situ observations at the SORPES
1014 station, *Journal of Geophysical Research: Atmospheres*, 120, 12679-12694,
1015 10.1002/2015jd023607, 2015.

1016 Xu, Z., Wang, T., Xue, L. K., Louie, P. K. K., Luk, C. W. Y., Gao, J., Wang, S. L., Chai, F. H.,
1017 and Wang, W. X.: Evaluating the uncertainties of thermal catalytic conversion in measuring
1018 atmospheric nitrogen dioxide at four differently polluted sites in China, *Atmos. Environ.*, 76,

1019 221-226, 10.1016/j.atmosenv.2012.09.043, 2013.

1020 Xu, Z., Wang, T., Wu, J., Xue, L., Chan, J., Zha, Q., Zhou, S., Louie, P. K. K., and Luk, C. W. Y.:
1021 Nitrous acid (HONO) in a polluted subtropical atmosphere: Seasonal variability, direct vehicle
1022 emissions and heterogeneous production at ground surface, *Atmos. Environ.*, 106, 100-109,
1023 10.1016/j.atmosenv.2015.01.061, 2015.

1024 Xu, Z., Huang, X., Nie, W., Chi, X., Xu, Z., Zheng, L., Sun, P., and Ding, A.: Influence of
1025 synoptic condition and holiday effects on VOCs and ozone production in the Yangtze River Delta
1026 region, China, *Atmos. Environ.*, 168, 112-124, 10.1016/j.atmosenv.2017.08.035, 2017.

1027 Xu, Z., Huang, X., Nie, W., Shen, Y., Zheng, L., Xie, Y., Wang, T., Ding, K., Liu, L., Zhou, D.,
1028 Qi, X., and Ding, A.: Impact of Biomass Burning and Vertical Mixing of Residual-Layer Aged
1029 Plumes on Ozone in the Yangtze River Delta, China: A Tethered-Balloon Measurement and
1030 Modeling Study of a Multiday Ozone Episode, *Journal of Geophysical Research: Atmospheres*,
1031 123, 11,786-711,803, 10.1029/2018jd028994, 2018.

1032 Yabushita, A., Enami, S., Sakamoto, Y., Kawasaki, M., Hoffmann, M. R., and Colussi, A. J.:
1033 Anion-Catalyzed Dissolution of NO₂ on Aqueous Microdroplets, *J. Phys. Chem. A*, 113,
1034 4844-4848, 10.1021/jp900685f, 2009.

1035 Ye, C., Zhou, X., Pu, D., Stutz, J., Festa, J., Spolaor, M., Tsai, C., Cantrell, C., Mauldin, R. L., 3rd,
1036 Campos, T., Weinheimer, A., Hornbrook, R. S., Apel, E. C., Guenther, A., Kaser, L., Yuan, B.,
1037 Karl, T., Haggerty, J., Hall, S., Ullmann, K., Smith, J. N., Ortega, J., and Knote, C.: Rapid cycling
1038 of reactive nitrogen in the marine boundary layer, *Nature*, 532, 489-491, 10.1038/nature17195,
1039 2016.

1040 Ye, C., Zhang, N., Gao, H., and Zhou, X.: Photolysis of Particulate Nitrate as a Source of HONO
1041 and NO_x, *Environ Sci Technol*, 51, 6849-6856, 10.1021/acs.est.7b00387, 2017.

1042 Yu, Y., Galle, B., Panday, A., Hodson, E., Prinn, R., and Wang, S.: Observations of high rates of
1043 NO₂-HONO conversion in the nocturnal atmospheric boundary layer in Kathmandu, Nepal,
1044 *ATMOSPHERIC CHEMISTRY AND PHYSICS*, 9, 6401-6415, 10.5194/acp-9-6401-2009, 2009.

1045 Zhou, L., Wang, W., Hou, S., Tong, S., and Ge, M.: Heterogeneous uptake of nitrogen dioxide on
1046 Chinese mineral dust, *J Environ Sci (China)*, 38, 110-118, 10.1016/j.jes.2015.05.017, 2015.

1047 Zhou, X., Civerolo, K., Dai, H., Huang, G., Schwab, J., and Demerjian, K.: Summertime nitrous
1048 acid chemistry in the atmospheric boundary layer at a rural site in New York State, *Journal of*
1049 *Geophysical Research: Atmospheres*, 107, ACH 13-11-ACH 13-11, 10.1029/2001jd001539, 2002.

1050 Zhou, X., Gao, H., He, Y., Huang, G., Bertman, S. B., Civerolo, K., and Schwab, J.: Nitric acid
1051 photolysis on surfaces in low-NO_x environments: Significant atmospheric implications,
1052 *Geophysical Research Letters*, 30, n/a-n/a, 10.1029/2003gl018620, 2003.

1053 Zhou, X., Zhang, N., TerAvest, M., Tang, D., Hou, J., Bertman, S., Alaghmand, M., Shepson, P.
1054 B., Carroll, M. A., Griffith, S., Dusanter, S., and Stevens, P. S.: Nitric acid photolysis on forest
1055 canopy surface as a source for tropospheric nitrous acid, *Nature Geoscience*, 4, 440-443,
1056 10.1038/ngeo1164, 2011.

Tables

Table 1. Sources and sinks for nitrous acid (HONO) in the troposphere.

Budget	Occurrence	Pathways	Abbr.
Sinks	Only daytime	$\text{HONO} + h\nu \xrightarrow{320-400\text{nm}} \text{OH} + \text{NO}$	R1
	Mainly daytime	$\text{HONO} + \text{OH} \rightarrow \text{NO}_2 + \text{H}_2\text{O}$	R2
	All day	Deposition / heterogeneous loss on aerosol	/
Sources	Mainly daytime	$\text{NO} + \text{OH} \xrightarrow{\text{M}} \text{HONO}$	R3
	Mainly nighttime	$2\text{NO}_{2(\text{g})} + \text{H}_2\text{O}_{(\text{ads})} \xrightarrow{\text{surf}} \text{HONO}_{(\text{g})} + \text{HNO}_{3(\text{ads})}$	R4
	Mainly daytime	$\text{NO}_{2(\text{g})} + \text{HC}_{\text{red}} \xrightarrow{\text{surf}} \text{HONO}_{(\text{g})} + \text{HC}_{\text{ox}}$	R5
	Only daytime	$\text{HNO}_3 / \text{NO}_3^- + h\nu \xrightarrow{\text{surf}} \text{HONO} / \text{NO}_2^- + \text{O}$	R6
	All day	Release of soil nitrite	/
	All day	Combustion emission (fossil and biomass)	/

Table 2. Overview of the measured HONO and NO_x levels in Nanjing and comparison with other urban or suburban sites.

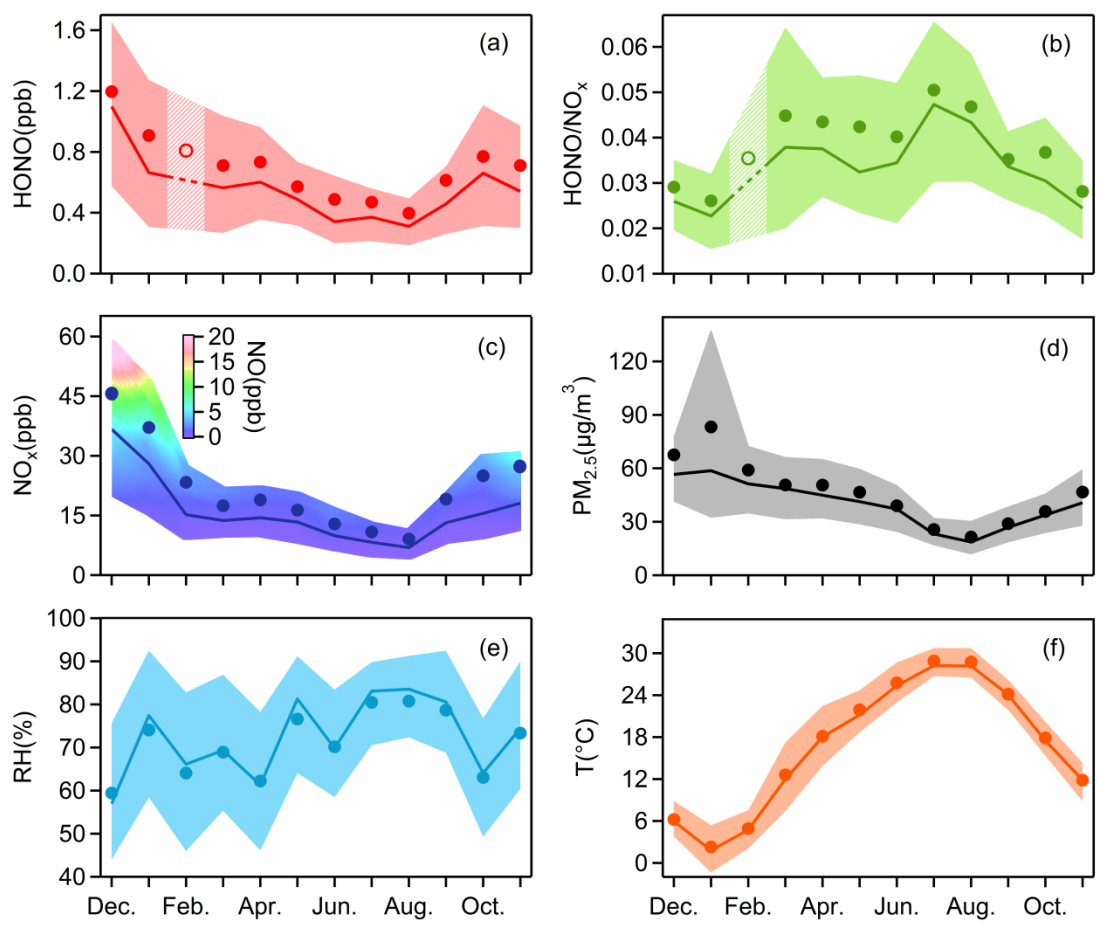
Location	Date	HONO(ppb)		NO ₂ (ppb)		NO _x (ppb)		HONO/NO ₂		HONO/NO _x		Ref
		Night	Day	Night	Day	Night	Day	Night	Day	Night	Day	
Rome(Italy)	May-Jun 2001	1.00	0.15	27.2	4.0	51.2	4.2	0.037	0.038	0.020	0.036	1
Kathmandu(Nepal)	Jan-Feb 2003	1.74	0.35	17.9	8.6	20.1	13.0	0.097	0.041	0.087	0.027	2
Tokto(Japan)	Jan-Feb 2004	0.80	0.05	31.8	18.2	37.4	26.3	0.025	0.003	0.021	0.002	3
Santiago(Chile)	Mar 2005	3.00	1.50	30.0	20.0	200.0	40.0	0.100	0.075	0.015	0.038	4
Mexico City(Mexico)	Mar 2006	/	0.43	/	28.4	/	44.8	/	0.015	/	0.010	5
Houston(USA)	Sep 2006	0.50	0.10	20.0	10.0	/	/	0.025	0.010	/	/	6
Shanghai(China)	Oct 2009	1.50	1.00	41.9	30.0	/	/	0.038	0.032	/	/	7
Hongkong(China)	Aug 2011	0.66	0.70	21.8	18.1	29.3	29.3	0.031	0.042	0.025	0.028	8
	Nov 2011	0.95	0.89	27.2	29.0	37.2	40.6	0.034	0.030	0.028	0.021	
	Feb 2012	0.88	0.92	22.2	25.8	37.8	48.3	0.036	0.035	0.025	0.020	
	May 2012	0.33	0.40	14.7	15.0	19.1	21.1	0.022	0.030	0.019	0.022	
Beijing(China)	Oct–Nov 2014	1.75	0.93	37.6	35.3	94.5	53.4	0.047	0.026	0.019	0.017	9
Xi'an(China)	Jul–Aug 2015	0.51	1.57	15.4	24.7	/	/	0.033	0.062	/	/	10
Jinan(China)	Sep–Nov 2015	0.87	0.66	25.4	23.2	38.0	37.5	0.049	0.034	0.034	0.022	11
	Dec 2015-Feb 2016	2.15	1.35	41.1	34.6	78.5	64.8	0.056	0.047	0.034	0.031	
	Mar–May 2016	1.24	1.04	35.8	25.8	47.3	36.0	0.046	0.052	0.035	0.041	
	Jun–Aug 2016	1.20	1.01	22.5	19.0	29.1	25.8	0.106	0.079	0.060	0.049	
Nanjing(China)	Nov 2017-Nov 2018	0.80	0.57	18.9	13.9	24.9	19.3	0.045	0.044	0.041	0.036	this study
	Dec-Feb(winter)	1.15	0.92	28.4	23.1	45.5	37.7	0.040	0.038	0.029	0.025	
	Mar–May(spring)	0.76	0.59	17.4	12.9	19.1	15.9	0.048	0.049	0.046	0.042	
	Jun–Aug(summer)	0.56	0.34	12.5	7.7	13.5	9.1	0.048	0.051	0.046	0.045	
	Sep–Nov(autumn)	0.81	0.51	18.9	13.4	25.1	17.7	0.044	0.035	0.039	0.029	

1: Acker et al. (2006); 2: Yu et al. (2009); 3: Kanaya et al. (2007); 4: Elshorbany et al. (2009); 5: Dusanter et al. (2009); 6: Wong et al. (2011); 7: Bernard et al. (2016); 8: Xu et al. (2015); 9: Tong et al. (2015); 10: Huang et al. (2017); 11: Li et al. (2018)

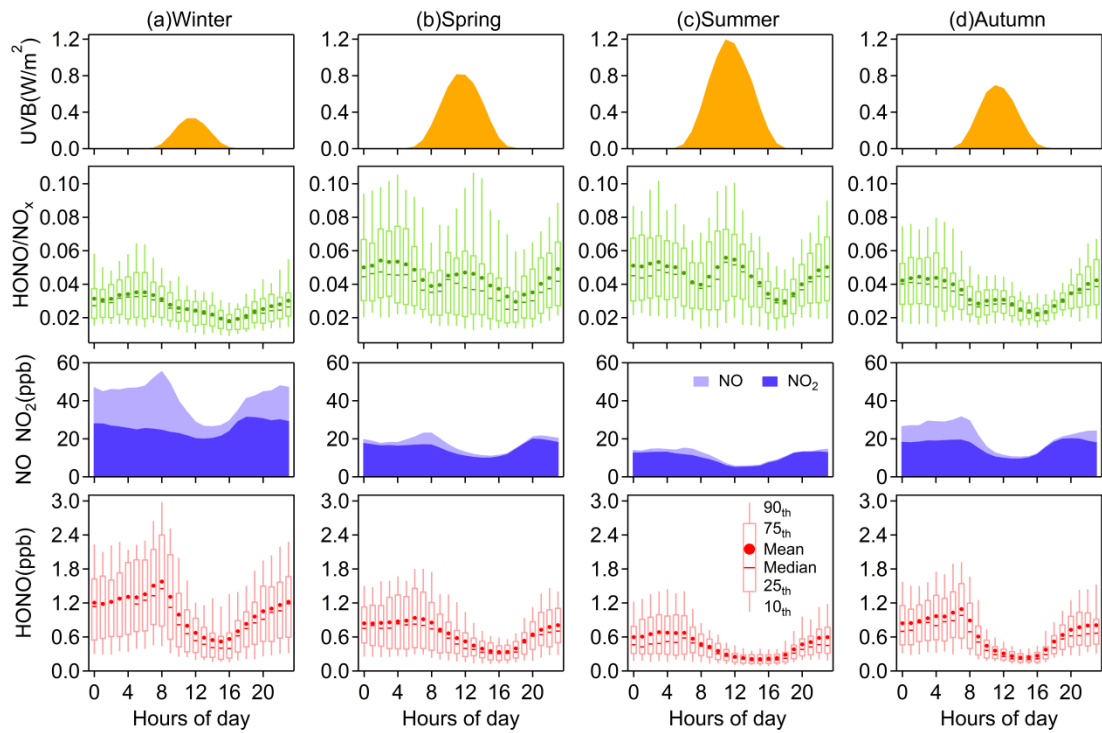
Table 3. Correlations of P_{unknown} against various parameters.

Parameters	Winter		Spring		Summer		Autumn	
	r	N	r	N	r	N	r	N
NO ₂	0.24	167	0.30	275	0.02	379	0.06	339
PM _{2.5}	0.21	167	0.40	275	0.16	379	0.20	339
NO ₃ ⁻	0.20	160	0.37	266	-0.05	366	0.12	336
SO ₄ ²⁻	0.16	154	0.27	266	0.07	370	0.19	329
NH ₄ ⁺	0.18	160	0.34	268	0.01	374	0.16	324
RH	0.00	167	-0.32	275	-0.33	379	-0.22	339
UVB	0.21	167	0.41	275	0.45	379	0.50	339
NO ₂ *PM _{2.5}	0.19	167	0.39	275	0.04	379	0.15	339
NO ₂ *NO ₃ ⁻	0.19	160	0.37	266	-0.08	366	0.11	336
NO ₂ *SO ₄ ²⁻	0.19	154	0.33	266	0.02	370	0.16	329
NO ₂ *NH ₄ ⁺	0.19	160	0.37	268	-0.02	374	0.13	324
UVB*NO ₂	0.33	167	0.62	275	0.41	379	0.59	339
UVB*PM _{2.5}	0.29	167	0.60	275	0.45	379	0.62	339
UVB*NO ₃ ⁻	0.26	160	0.51	266	0.18	366	0.41	336
UVB*SO ₄ ²⁻	0.19	154	0.46	266	0.36	370	0.54	329
UVB*NH ₄ ⁺	0.23	160	0.49	268	0.27	374	0.49	324
NO ₂ *UVB*PM _{2.5}	0.24	167	0.58	275	0.30	379	0.48	339

1057 **Figures**
 1058

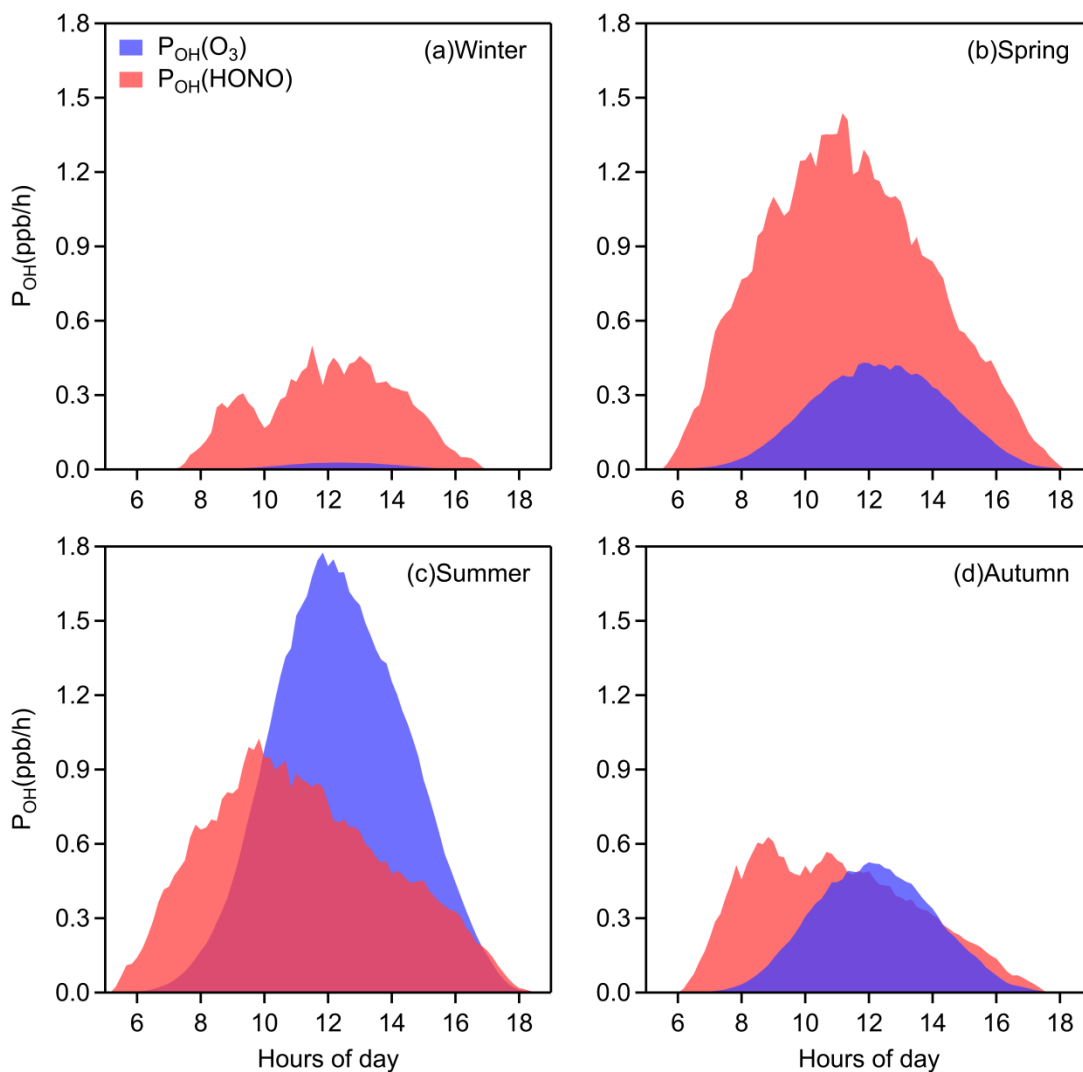


1059
 1060 **Fig. 1.** Monthly variations of (a) HONO, (b) HONO/NO_x, (c) NO_x, (d) PM_{2.5}, (e) RH and (f) T.
 1061 The solid bold lines are median values, the markers indicate mean values, and the shaded areas
 1062 represent percentiles of 75% and 25%. In (a) and (b), values in February are linearly interpolated
 1063 based on the data from the months before and after, since there were only few days when HONO
 1064 was observed in February. In (c), the shaded area is colored by the 25th to the 75th percentiles of
 1065 NO.
 1066



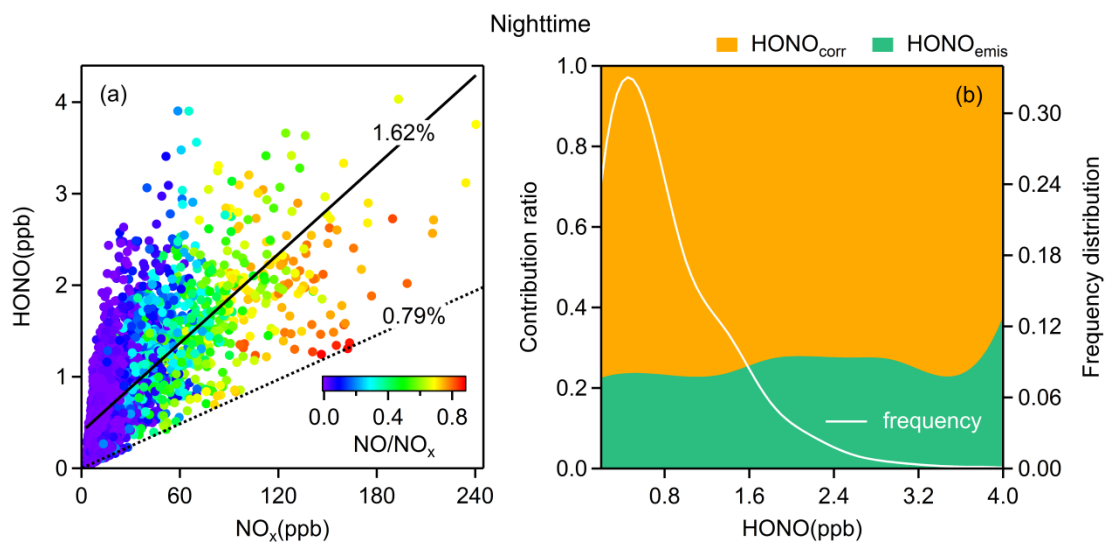
1067
 1068
 1069
 1070

Fig. 2. Diurnal variations of HONO, NO, NO₂, HONO/NO_x, UVB in (a) winter, (b) spring, (c) summer, (d) autumn. NO, NO₂ and UVB values are displayed as their mean concentrations.



1071
 1072
 1073
 1074
 1075
 1076
 1077
 1078
 1079
 1080

Fig. 3. Averaged OH production rates from photolysis of HONO and ozone in (a) winter, (b) spring, (c) summer, and (d) autumn. The P_{OH}(HONO) here is actually the net OH production rate, by subtracting the consumption of OH radicals by R2 and R3. The mean values of P_{OH}(HONO) at daytime (08:00-16:00 LT) are: 0.29 ppb/h in winter, 0.97 ppb/h in spring, 0.68 ppb/h in summer, 0.42 ppb/h in autumn.



1081

1082 **Fig. 4.** (a) The relationship between HONO and NO_x colored by NO/NO_x. The dotted line is the
 1083 emission ratio derived in this study and the solid line is obtained from simple linear fitting; (b)
 1084 average emission contribution ratios for different concentrations of HONO and the frequency
 1085 distribution of HONO concentrations. Both (a) and (b) are nighttime values.

1086

1087

1088

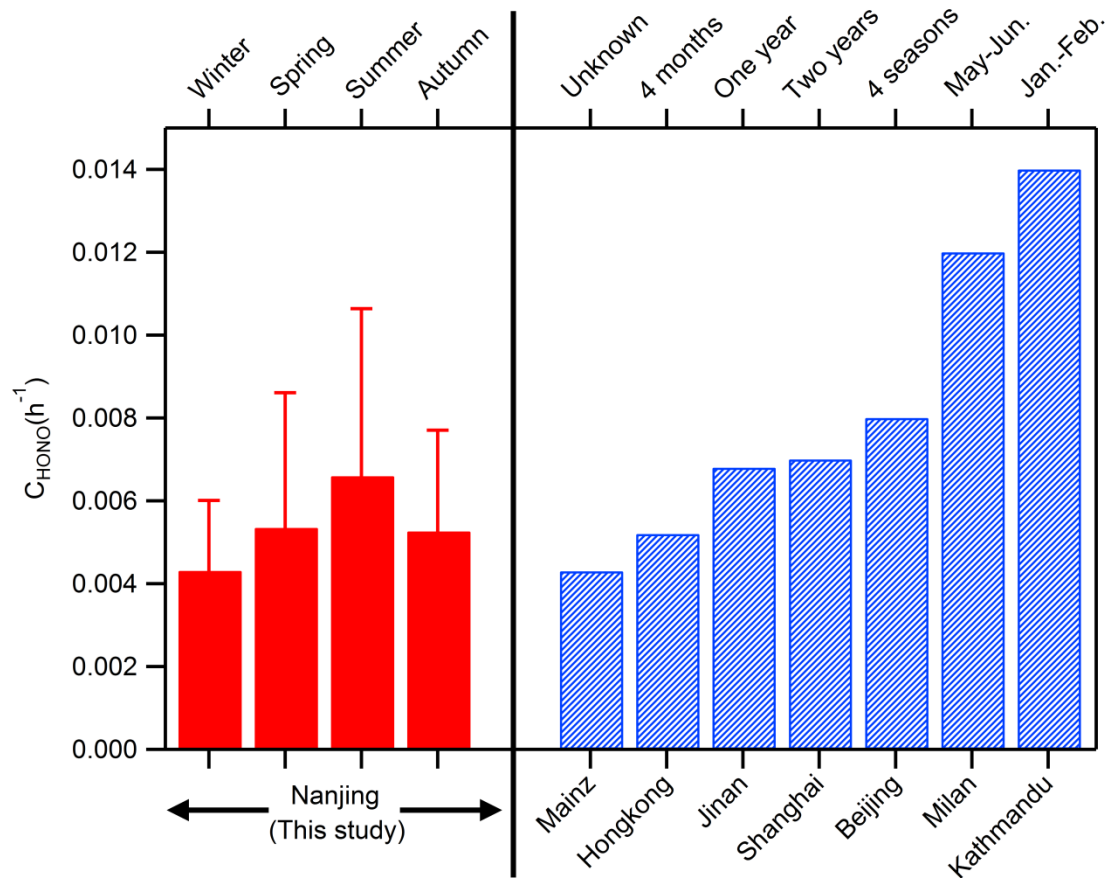
1089

1090

1091

1092

1093



1094

Fig. 5. Comparison of observed NO₂ to HONO conversion rates in cities: Nanjing (this study); Mainz (Lammel, 1999); Hongkong (Xu et al., 2015); Jinan (Li et al., 2018); Shanghai (Wang et al., 2013); Beijing (Wang et al., 2017); Milan (Alicke et al., 2002); and Kathmandu (Yu et al., 2009).

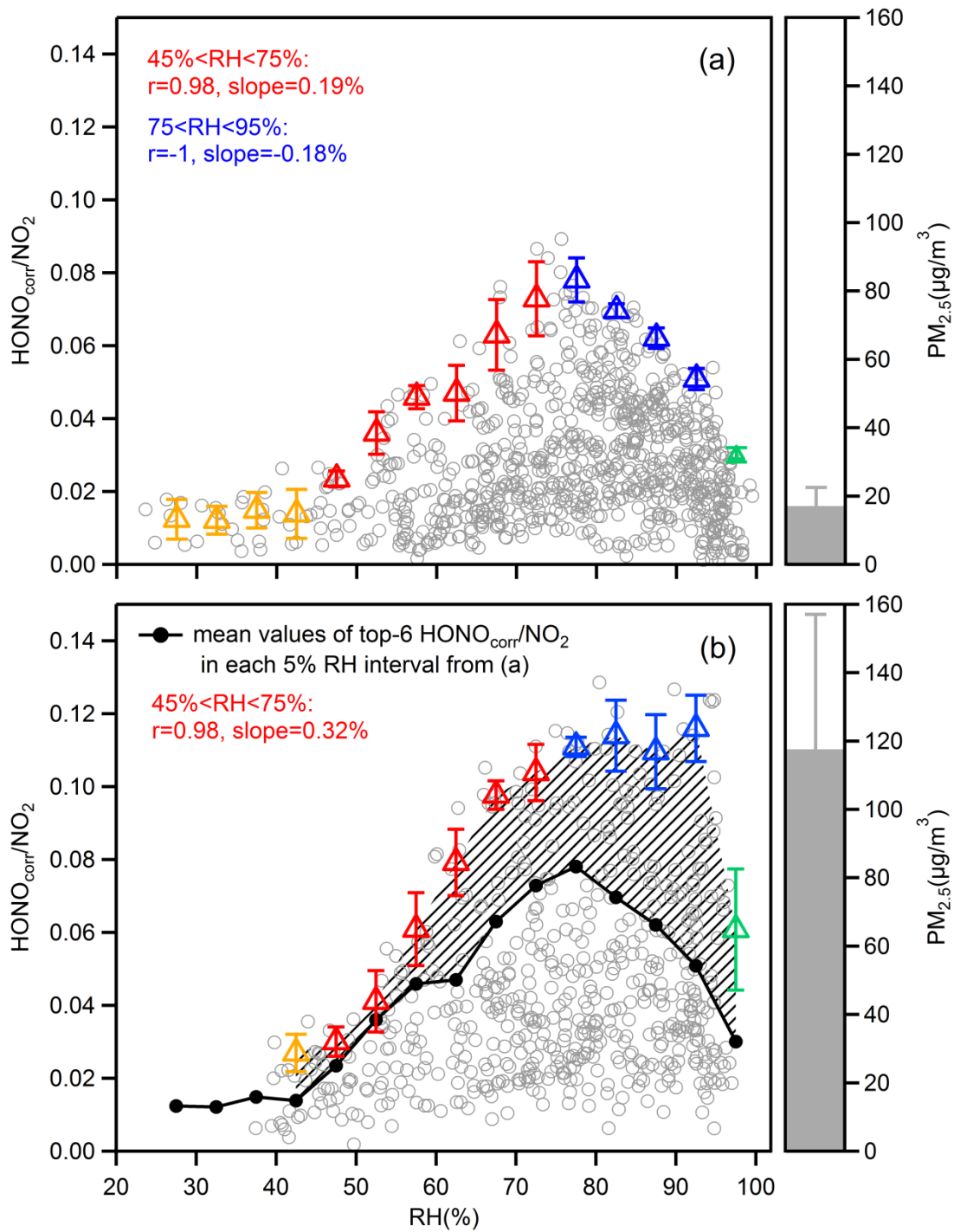


Fig. 6. Scatter plot of $\text{HONO}_{\text{corr}}/\text{NO}_2$ and RH during nighttime, separating the data into (a) clean hours (hourly mean $\text{PM}_{2.5} < 25 \mu\text{g}/\text{m}^3$) and (b) polluted hours (hourly mean $\text{PM}_{2.5} > 75 \mu\text{g}/\text{m}^3$). Triangles are the averaged top-6 $\text{HONO}_{\text{corr}}/\text{NO}_2$ in each 5% RH interval, and the error bars are the standard deviations. The overall average concentrations of $\text{PM}_{2.5}$ in (a) and (b) are shown to the right of the figures.

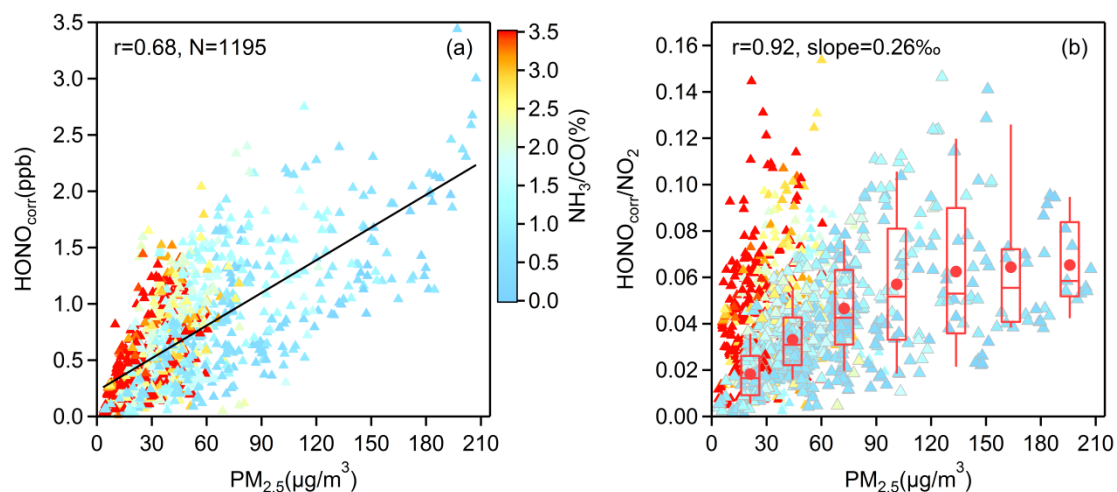


Fig. 7. (a) The correlation between $\text{HONO}_{\text{corr}}$ and $\text{PM}_{2.5}$, and (b) the correlation between $\text{HONO}_{\text{corr}}/\text{NO}_2$ and $\text{PM}_{2.5}$, all scatters come from the time (3:00–6:00 LT) when $\text{HONO}_{\text{corr}}/\text{NO}_2$ reaches the pseudo steady state at each night and are colored by NH_3/CO . In (b), the larger triangles with gray borders, depict the measured data from November to May, and the boxplot in each $30 \mu\text{g}/\text{m}^3$ interval of $\text{PM}_{2.5}$ is illustrated according to the same data, the red box boundaries represent interquartile range, the whiskers represent the 10%–90% percentile range, the horizontal red lines represent median values and the red markers represent mean values. The correlation coefficient and the slope of the linearly fitted line in (b) are derived from the average $\text{HONO}_{\text{corr}}/\text{NO}_2$ and average $\text{PM}_{2.5}$ in each box.

1095

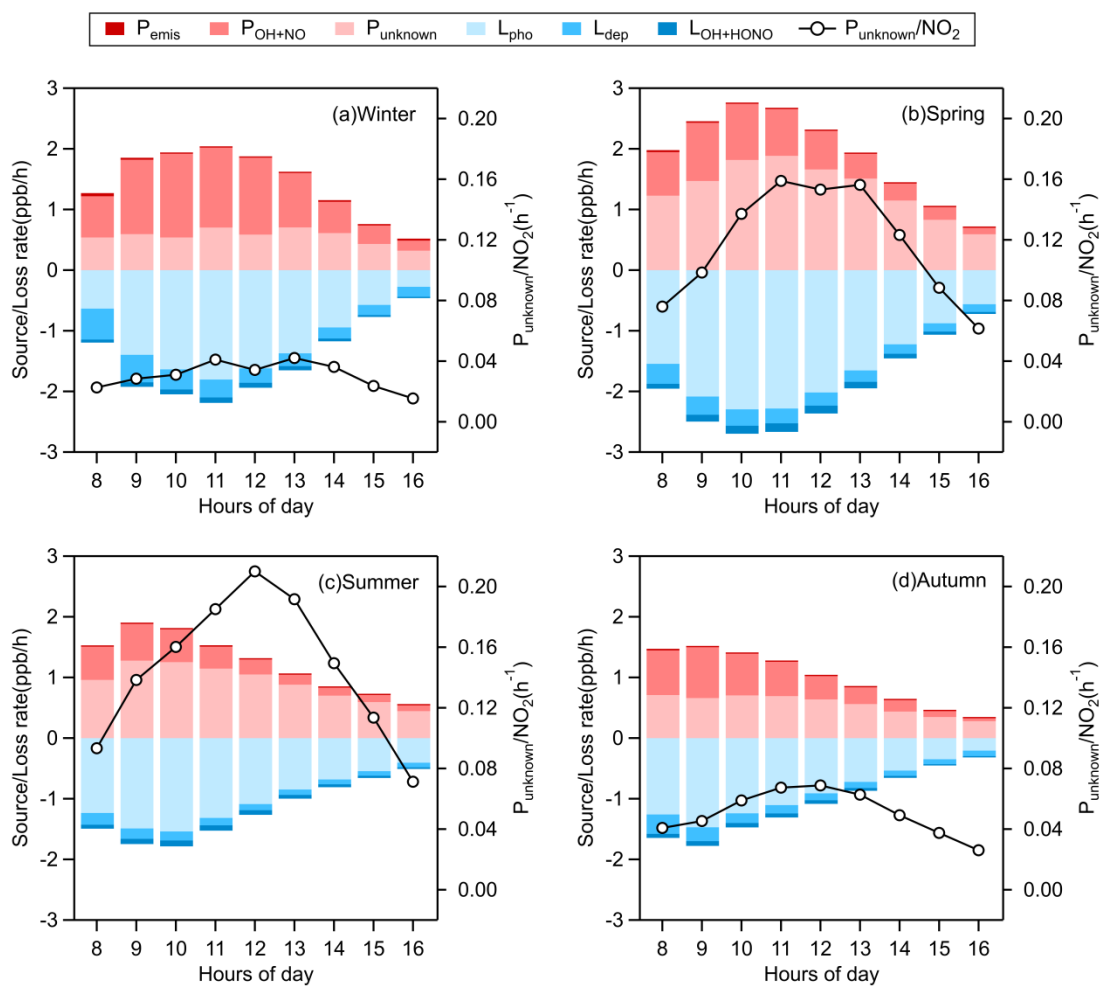


Fig. 8. Averaged daytime HONO budget and the missing source strength (P_{unknown}) normalized by NO_2 in (a) winter, (b) spring, (c) summer, and (d) autumn. The mean values of P_{unknown} at noontime (10:00-14:00 LT) are: 0.58 ppb/h in winter, 1.72 ppb/h in Spring, 1.11 ppb/h in summer, 0.66 ppb/h in autumn.

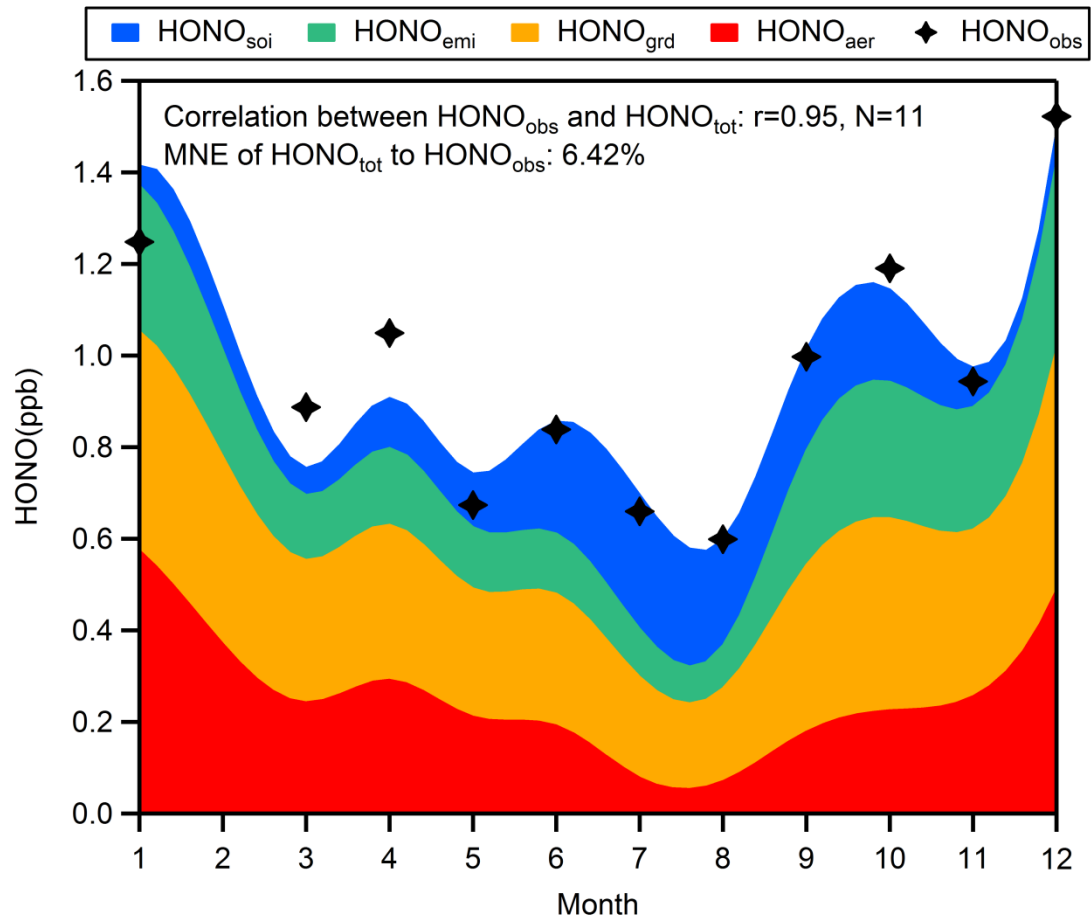


Fig. 9. Seasonal variations of 4 sources of mean HONO at night (3:00-6:00 LT). The mean normalized error (MNE) of HONO_{tot} to HONO_{obs} is 6.42%.